JGR Atmospheres

RESEARCH ARTICLE
10.1029/2019JD031207

Modeling the Sources and Transport Processes During Extreme Ammonia Episodes in the U.S. Corn Belt

Cheng Hu[1,2], Timothy J. Griffis[1], John M. Baker[1,3], Jeffrey D. Wood[4], Dylan B. Millet[1], Zhongjie Yu[1], and Xuhui Lee[5,6]

[1]Department of Soil, Water, and Climate, University of Minnesota, Twin Cities, St. Paul, MN, USA, [2]College of Biology and the Environment, Joint Center for sustainable Forestry in Southern China, Nanjing Forestry University, Nanjing, China, [3]U.S. Department of Agriculture, Agriculture Research Service, St. Paul, MN, USA, [4]School of Natural Resources, University of Missouri, Columbia, MO, USA, [5]School of Forestry and Environmental Studies, Yale University, New Haven, CT, USA, [6]Yale-NUIST Center on Atmospheric Environment, International Joint Laboratory on Climate and Environment Change (ILCEC), Nanjing University of Information, Science and Technology, Nanjing, China

Abstract Atmospheric ammonia (NH_3) is the primary form of reactive nitrogen (N_r) and a precursor of ammonium (NH_4^+) aerosols. Ammonia has been linked to adverse impacts on human health, the loss of ecosystem biodiversity, and plays a key role in aerosol radiative forcing. The midwestern United States is the major NH_3 source in North America because of dense livestock operations and the high use of synthetic nitrogen fertilizers. Here, we combine tall-tower (100 m) observations in Minnesota and Weather Research and Forecasting model coupled with Chemistry (WRF-Chem) modeling to investigate high and low NH_3 emission episodes within the U.S. Corn Belt to improve our understanding of the distribution of emission sources and transport processes. We examined observations and performed model simulations for cases in February through November of 2017 and 2018. The results showed the following: (1) Peak emissions in November 2017 were enhanced by above-normal air temperatures, implying a Q_{10} (i.e., the change in NH_3 emissions for a temperature increase of 10°C) of 2.5 for emissions. (2) The intensive livestock emissions rom northern Iowa, approximately 400 km away from the tall tower, accounted for 17.6% of the abundance in tall-tower NH_3 mixing ratios. (3) Ammonia mixing ratios in the innermost domain 3 frequently (i.e., 336 hr, 48% of November 2017) exceeded 5.3 ppb, an important air quality health standard. (4) In November 2017, simulated NH_3 net ecosystem exchange (the difference between NH_3 emissions and dry deposition) accounted for 60–65% of gross NH_3 emissions for agricultural areas and was 2.8–3.1 times the emissions of forested areas. (5) We estimated a mean annual NH_3 net ecosystem exchange of 1.60 ± 0.06 nmol $\cdot$ $m^{-2} \cdot s^{-1}$ for agricultural lands and -0.07 ± 0.02 nmol $\cdot$ $m^{-2} \cdot s^{-1}$ for forested lands. These results imply that future warmer fall temperatures will enhance agricultural NH_3 emissions, increase the frequency of dangerous NH_3 episodes, and enhance dry NH_3 deposition in adjacent forested lands.

Key Points:
- Peak emissions in November 2017 were enhanced by above-normal air temperatures, implying a Q_{10} for emissions of 2.5
- The intensive livestock emissions from northern Iowa accounted for 17.5% of the abundance in tall-tower NH3 mixing ratios
- We estimated a mean annual NH3 NEE of 1.60 nmol $\cdot$ $m^{-2} \cdot s^{-1}$ for agricultural lands and −0.07 nmol $\cdot$ $m^{-2} \cdot s^{-1}$ for forested land

Supporting Information:
- Supporting Information S1

Correspondence to:
C. Hu and T. J. Griffis,
huxxx991@umn.edu;
timgriffis@umn.edu

Citation:
Hu, C., Griffis, T. J., Baker, J. M., Wood, J. D., Millet, D. B., Yu, Z., & Lee, X. (2020). Modeling the sources and transport processes during extreme ammonia episodes in the U.S. Corn Belt. *Journal of Geophysical Research: Atmospheres*, *125*, e2019JD031207. https://doi.org/10.1029/2019JD031207

Received 20 JUN 2019
Accepted 19 DEC 2019
Accepted article online 22 DEC 2019

Author Contributions:
Funding acquisition: Timothy J. Griffis, John M. Baker, Jeffrey D. Wood
Investigation: Zhongjie Yu
Project administration: Timothy J. Griffis, John M. Baker, Jeffrey D. Wood
Supervision: Timothy J. Griffis, John M. Baker, Dylan B. Millet, Xuhui Lee
Writing - original draft: Cheng Hu

©2019. American Geophysical Union. All Rights Reserved.

1. Introduction

Atmospheric ammonia (NH_3) is the primary form of reactive nitrogen (N_r) and a precursor of ammonium (NH_4^+) aerosols via chemical reactions with sulfuric (H_2SO_4) and nitric (HNO_3) acids (Erisman et al., 2008; Galloway et al., 2008; Li et al., 2016). Ammonium aerosols form the dominant inorganic component in fine particulate matter (i.e., particulate matter [PM] 2.5) and have a significant influence on radiative scattering, cloud formation, and human health (Warner et al., 2017). Although both gaseous NH_3 and ammonium particles are short-lived species, with lifetimes varying between a few hours and a few weeks, they can lead to eutrophication and soil acidification by atmospheric transport (tens to hundreds of kilometers from the source) and dry/wet deposition to sensitive natural ecosystems (Dragosits et al., 2002; Makar et al., 2015; Stevens, 2019). Excessive reduced nitrogen NH_x (NH_3 and NH_4^+) can also be transported by runoff and drainage waters and lead to river acidification, algal blooms, and biodiversity loss in aquatic systems (Erisman et al., 2008; Hellsten et al., 2008).

The main NH_3 sources include agriculture, industry, and biomass burning, with over 80% from anthropogenic sources globally (Butler et al., 2016; Sutton et al., 2013). In the United States, 84% of the anthropogenic NH_3 emissions are attributed to agricultural categories with 30% attributed to fertilizer volatilization and 54% to livestock production (Butler et al., 2016). The U.S. Corn Belt has been identified as a global NH_3

hotspot driven by intense agricultural activity including significant use of synthetic nitrogen fertilizers and highly concentrated animal feedlots (Shephard et al., 2011; Yu et al., 2018). For example, Iowa and Minnesota accounted for approximately 50% of national hog production in 2018 according to the U.S. Department of Agriculture (USDA Annual Report, 2018, https://www.statista.com/statistics/194371/top-10-us-states-by-number-of-hogs-and-pigs/). Ammonia dry deposition downwind of these intensive agricultural areas can dominate the total N_r load from the atmosphere (Li et al., 2016, 2017) and potentially have significant input to the nitrogen load of natural ecosystems via atmospheric and river transport (Ellis et al., 2013).

In the Upper Midwest, direct observations indicate that both dry and total deposition rates of nitrogen (i.e., NH_3, NH_4^+, NO_3^-, and HNO_3) are higher than anywhere else in the United States (Li et al., 2016). Dry deposition of NH_3 plays a dominant role and estimated to account for around 50% and 80% for the total and dry N deposition in Upper Midwest, respectively (Li et al., 2016). For these reasons, robust estimation of NH_3 emissions from these agricultural regions is essential for air quality modeling, quantifying its environmental impacts, and developing NH_3 mitigation strategies.

The uncertainty of NH_3 emission estimates for the U.S. Corn Belt remains relatively high compared to other reactive nitrogen species (i.e., N_2O) or other pollutants such as NO_x or SO_2. The high uncertainty is attributed to the overall lack of observations and the difficulty associated with measuring NH_3 fluxes (Reis et al., 2009; Sutton et al., 2013). Short-term weather variations and lack of detailed crop cultivation information, including fertilizer types and application practices, heterogeneity in land management activities, and the dynamic bidirectional NH_3 flux, are important factors contributing to these large and persistent NH_3 emission uncertainties (Lonsdale et al., 2017; Nowak et al., 2012). Further, since NH_3 is not yet a regulated pollutant in the United States, there has been less emphasis related to reducing its uncertainty (Paulot et al., 2014).

Ammonia emission inventories, based on the Intergovernmental Panel on Climate Change (IPCC) methodology (IPCC, 2013), make use of activity data and emission factors (EFs) and have been applied broadly in calculating gross NH_3 emissions. Available NH_3 inventories include EDGAR (Emission Database for Global Atmospheric Research, Olivier et al., 1994) and NEI (National Emission Inventory, Reis et al., 2009). Large biases have been reported for these NH_3 inventories. For example, NEI was found to underestimate by a factor of 2.7 in Colorado (Battye et al., 2016). By comparing with satellite and ground NH_3 concentration observations, NH_3 inventories were found to be underestimated by 2 to 4 times in California (Heald et al., 2012; Lonsdale et al., 2017; Nowak et al., 2012; Zhu et al., 2015). Although some empirical scaling factors (i.e., monthly) were applied (Paulot et al., 2014; Zhang et al., 2012), the magnitude and seasonality of NH_3 emissions are also found with large biases in the U.S. Midwest; a priori EDGAR monthly NH_3 inventories peaked in summer following volatilization in high-temperature conditions, while a recent study concluded that it should have a higher peak in spring due to corn fertilization (Paulot et al., 2014). It is important to note that constant EFs are applied in most inventories as a simplification. However, it is well established that these emissions are highly dependent on environmental factors such as air temperature and can vary dramatically on short time scales (Sutton et al., 2013; Zhang et al., 2017). Further, some studies have shown that the use of online temperature-dependent NH_3 emissions can significantly improve simulated NH_3 mixing ratios (Warner et al., 2017).

Measurements of NH_3 emissions from agricultural sources remain challenging and are relatively rare through the U.S. and other major agricultural regions of the world. Measurement approaches have included chambers (Aneja et al., 2000; Parker et al., 2013), eddy covariance (Ferrara et al., 2012, 2016; Sun et al., 2015), relaxed eddy-accumulation (Nelson et al., 2017, 2019; Zhu et al., 2000), flux-gradients (Nelson et al., 2019; Phillips et al., 2004), and satellite-based remote sensing (Lonsdale et al., 2017; Zhu et al., 2013). Direct measurements of agricultural NH_3 emissions have shown high sensitivity to climate (Skjøth & Geels, 2013; Sutton et al., 2013; Zhang et al., 2017). Ammonia emissions are thought to increase exponentially as a function of air temperature (Riddick et al., 2016). In principle, the NH_3 volatilization rate can double with a temperature increase of 5°C, equivalent to a Q_{10} of 3 to 4 (Sutton et al., 2013). Many studies have tried to quantify the temperature sensitivity of NH_3 emissions and have reported Q_{10} values ranging between 1.25 and 10 for different NH_3 sources and climate zones (Hensen et al., 2009; Sutton et al., 2013; Zhang et al., 2017). Other field-based studies have also reported that agricultural NH_3 EFs show large seasonal variability, with summer EFs 2 to 5 times larger than for winter (McGinn et al., 2007; Yang et al., 2016).

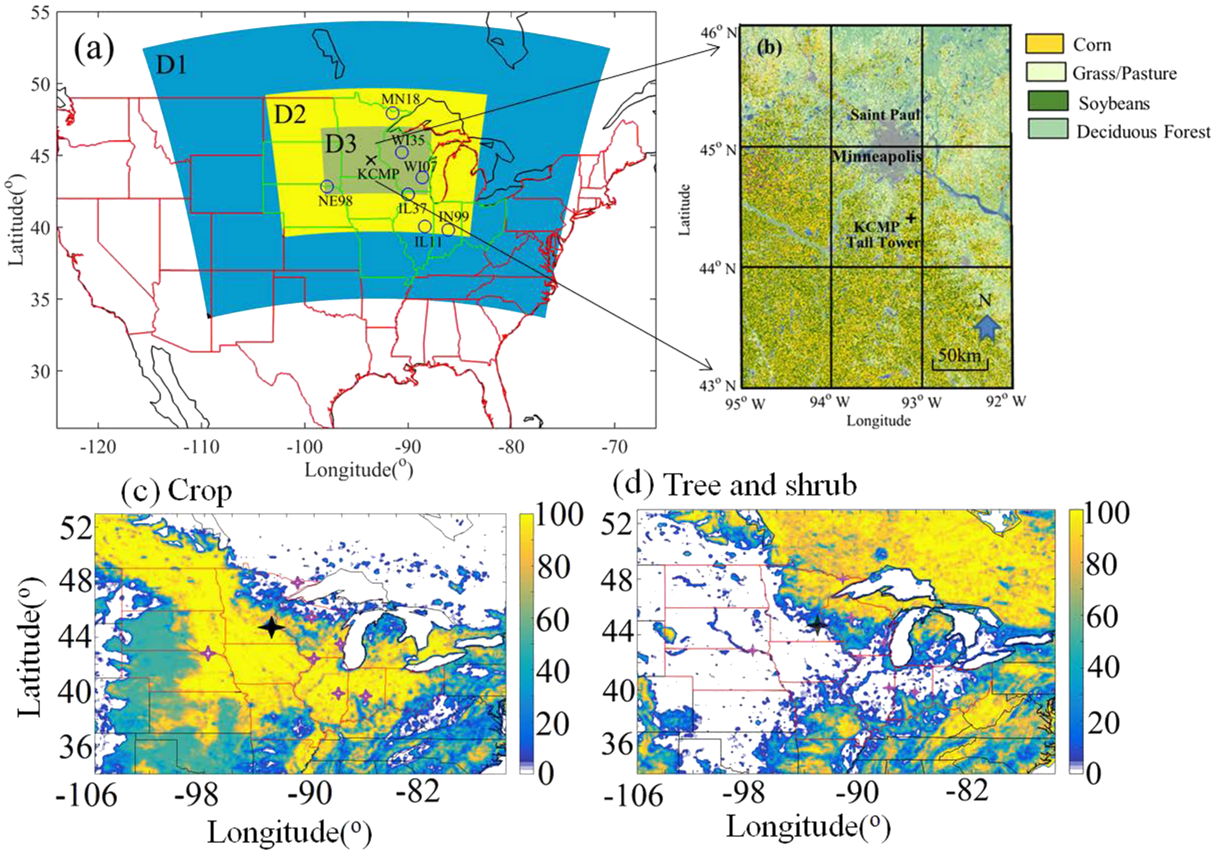

Figure 1. Maps of (a) three domain setups used in Weather Research and Forecasting model coupled with Chemistry (WRF-Chem) model: the 10 states represent U.S. Corn Belt is bounded by a green line; (b) land use categories and urban areas; (c) the percent plant functional types (PFTs) for crops; and (d) tree and shrub. Note that the additional purple symbols in c and d are the locations of monitoring stations appearing in Table 1, and black "x" indicate tall tower site.

The NH_3 concentration observations reported in previous studies have largely been obtained using ground-level passive samplers for its relatively low instrumentation and technical requirements, such as those used at the Ammonia Monitoring Network (AMoN) sites (National Atmospheric Deposition Program [NADP], 2017). These data have provided important information on regional NH_3 concentration distributions and shed light on potential NH_3 hotspots (Yu et al., 2018). However, these ground-level passive samplers have a very limited source footprint and very low temporal resolution, and large uncertainties have been reported when using these data to estimate dry deposition fluxes (Schrader et al., 2018). Further, they are not ideal for measuring vertical gradients of NH_3, which can lead to difficulty in interpreting near-surface observations from a single sampling altitude. Some passive samplers have been used to measure vertical NH_3 profiles (Zhang et al., 2018) in order to estimate NH_3 net ecosystem exchange (hereafter NH_3 net ecosystem exchange [NEE]). Unfortunately, these measurements have relatively low temporal resolution, from weekly to biweekly, and therefore cannot characterize shorter-term emission changes that are needed to understand the underlying processes (i.e., short-term weather variability or land management activities).

Ammonia measurements at finer time scales that can better characterize the full atmospheric boundary layer are needed to evaluate model performance, emission inventory uncertainties, and to provide deeper insights regarding NH_3 source/sink behavior and regional transport. Only a few studies have reported hourly NH_3 profiles using tall towers (i.e., 160 and 280 m) in the Netherlands (Dammers et al., 2017) and Colorado, USA (Li et al., 2017; Tevlin et al., 2017). Here, we build on our previous tall tower NH_3 work conducted within the U.S. Corn Belt (Griffis et al., 2019) by using the Weather Research and Forecasting model coupled with Chemistry (WRF-Chem) model to assess the regional sinks, sources, and transport processes associated with high NH_3 emission events.

The objectives of this study therefore were to (1) compare observed and modeled hourly NH_3 mixing ratios and evaluate NH_3 inventories at the hourly to monthly time-scales, (2) examine the NH_3 emissions and transport processes associated with high NH_3 emission episodes and secondary $PM_{2.5}$ formation, and (3) quantify the NH_3 NEE by accounting for both NH_3 dry deposition and gross emissions from land surfaces within the U.S. Corn Belt including agricultural and natural ecosystems.

2. Materials and Methods

2.1. Research Site

The main research site is the tall (244-m height) tower trace gas observatory (KCMP radio tower, 44.69°N, 93.07°W), located about 25 km south of the Minneapolis-Saint Paul metropolitan area (Figure 1**)**. Our previous work has shown that the land use surrounding the tall tower for a radius extending to 300 km consists of cropland, forest, and grass/pasture occupying 40%, 25%, and 21%, respectively (Hu et al., 2018). Past work at this site has examined surface-atmosphere fluxes of CO_2 (Griffis et al., 2010; Hu et al., 2018), CH_4 (Chen et al., 2018; Zhang et al., 2014), N_2O (Chen et al., 2016; Griffis et al., 2017), H_2O (Griffis et al., 2016), CO, and VOCs (Hu et al., 2015; Kim et al., 2013). Further details about the research facility and study site can be found in Griffis et al. (2013).

2.2. Ammonia, Aerosol, and Meteorology Observations

Two sets of NH_3 mixing ratio observations were used in this study. First, NH_3 mixing ratios were measured at 1-Hz frequency from the 56- and 100-m levels of the KCMP tall tower using an off-axis cavity ring-down spectrometer (Model EAA-30-EP, Los Gatos Research, San Jose, CA, USA; Griffis et al., 2019). Ammonia mixing ratio measurements were initiated on 21 March 2017 and are ongoing as of 15 December 2019. These high-frequency data were block averaged at hourly intervals for comparison with the WRF-Chem model results. The manufacturer-reported NH_3 mixing ratio uncertainty (1 σ) is less than 0.2 ppb for an integration period of 100 s. Calibrations performed under field conditions showed that the Allan deviation was 0.24 ppb for an integration period of 100 s (Griffis et al., 2019).

The second set of NH_3 mixing ratio observations were obtained from AMoN sites (http://nadp.slh.wisc.edu/data/AMoN/). These sites provide ground-level observations with broad spatial coverage across the United States at biweekly temporal resolution and have been available since 2007. AMoN data have been used in the past to assess NH_3 trends and for model evaluation (Butler et al., 2016; Paulot et al., 2014; Yu et al., 2018). The ground-level NH_3 mixing ratio measurements use Radiello passive samplers (http://www.radiello.com); previous studies have found that these have a mean relative bias of −9% compared with annular denuder systems and a precision of 5% (Puchalski et al., 2011, 2015).

Four of the AMoN sites are located within our innermost nested model domain (D3; see Figure 1), while three sites are within our intermediate nested domain (D2). Site and model domain details are provided in Figure 1, Table 1, and section 2.3. These seven sites are located in four different land use regions including crop land (WI35, IL37, and IL11), livestock (NE98), remote or background sites (WI07 and MN18), and Urban (IN99). The AMoN sites used here thus represent a diversity of NH_3 emission characteristics within the U.S. Corn Belt for comparisons with our model results.

Fine particle ($PM_{2.5}$ mass) observations within the Minneapolis-Saint Paul metropolitan area (Table 2) were also used to evaluate the WRF-Chem model performance. These data were provided by the U.S. Environmental Protection Agency (EPA) air quality system (https://aqs.epa.gov/api). Such data have been widely used to evaluate atmospheric model performance (Hu et al., 2013; Yegorova et al., 2011; Zhu et al., 2018). Supporting meteorological data including wind direction (WD), wind speed (WS), 2-m air temperature (T_2), and relative humidity (RH) were measured at the US-Ro1 Ameriflux site, which is located within 5 km of the KCMP tall tower. Three additional Ameriflux sites, including Ro4, Ro5, and Ro6, were also used to evaluate T_2. Planetary boundary layer (PBL) height observations (seasonal average from November to February) were obtained at a nearby site (~20-km distance) in 2009 and used to compare with our model simulations given the lack of direct observations during our study period. The 3-hourly NARR (North American Regional Reanalysis) PBL heights reanalysis were also used.

Table 1
NH_3 Observation Sites (Including AMoN Sites and KCMP Tall Tower) and EPA $PM_{2.5}$ Site Information

Site ID	State	Latitude (°)	Longitude (°)	Elevation (m)	Model domain	Land use
KCMP	MN	44.69	−93.07	290	Domain3	Agriculture
WI35	WI	45.21	−90.60	472	Domain3	Agriculture
NE98	NE	42.83	−97.85	443	Domain3	Agriculture (Range)
IL37	IL	42.29	−90.00	274	Domain3	Agriculture
WI07	WI	43.47	−88.62	287	Domain3	Remote
MN18	MN	47.95	−91.50	524	Domain2	Remote
IL11	IL	40.05	−88.37	212	Domain2	Agriculture
IN99	IN	39.81	−86.11	230	Domain2	Urban
Apple Valley	MN	44.75	−93.20	305	Domain3	Urban
Ben Franklin School	MN	44.00	−92.45	/	Domain3	Urban
Harding High School	MN	44.96	−93.04	296	Domain3	Urban
Talahi School	MN	45.55	−94.13	/	Domain3	Urban
St. Michael School	MN	45.21	−93.67	288	Domain3	Urban

Abbreviations: EPA: Environmental Protection Agency; $PM_{2.5}$: particulate matter 2.5.

2.3. WRF-Chem Model Setup

The WRF-Chem model (version 3.9.1.1) simulations used three nested domains with spatial resolutions of 45, 15, and 5 km, respectively (Figure 1). The intermediate 15-km domain (D2) contained the majority of the U.S. Corn Belt including 10 states (Chen et al., 2018). The innermost 5-km domain (D3) included Northern Iowa (a hotspot for NH_3 livestock emissions) and southern Minnesota, which is dominated by agricultural lands. Comparisons of average NH_3 emissions, NH_3 mixing ratios, NH_3 dry deposition velocity (V_d), and NH_3 dry deposition fluxes were conducted based on different land use classifications, where the percent coverage for 25 plant functional types was provided by CLM45-BGC (Community Land Model coupled to Biogeochemistry) with a spatial resolution of 0.125° (Oleson et al., 2013). As shown in Figures 1b and 1c, we aggregated land use into two different categories: crops and tree/shrub (the latter is referred to hereafter as forested area) to represent agricultural and natural ecosystems. To better evaluate uncertainties associated with different land uses, model results were compared across varying coverage thresholds of 70%, 80%, and 90% to define these two different land surfaces (see results in section 3.5). As shown in Figure 1, the tall tower observations can provide important information regarding the atmospheric transport of NH_3 from both managed agricultural lands (predominantly lying to the south and east) and natural ecosystems (to the north and west), which provides a unique opportunity to quantify anthropogenic emissions and deposition for both managed and natural ecosystems.

All three model domains have 36 vertical layers extending from the land surface to a height of 20 km, corresponding to a pressure height of 50 hPa. This includes eight additional layers we added below 100 m

Table 2
Descriptions of Eight Different NH_3 Emission Cases in WRF-Chem Model

Case number	NH_3 sources	Details for NH_3 emissions	Time period	Spatial resolution	NH_3 emissions in domain 3 ($nmol \cdot m^{-2} \cdot s^{-1}$)
Case1	NEI 2011	Diurnal variations	November 2017	4 km	3.23
Case2	NEI 2011	Constant (no diurnal variations)	November 2017	4 km	3.23
Case3	NEI 2017	Scaled NEI 2011 to 2017	November 2017	4 km	2.18
Case4	NEI 2017	Zero North Iowa State	November 2017	4 km	1.50
Case5	NEI 2017	Zero domains 2 and 3	November 2017	4 km	0
Case6	EDGAR	Diurnal variations	November 2017	0.1°	1.75
Case7	NEI 2011,2017, EDGAR	Same as Cases 1, 5, and 6	November 2018	0.1° and 4 km	1.75–3.23
Case8	NEI 2017	Scale NEI 2011 to 2017	2017	4 km	2.18

Abbreviations: EDGAR: Emission Database for Global Atmospheric Research; NEI: National Emission Inventory; WRF-Chem: Weather Research and Forecasting model coupled with Chemistry.

to improve the simulation of NH_3 in terms of its vertical transport and gas-particle phase partitioning. Specifically, levels were added at vertical intervals of 10–20 m, including two with midpoints at 100- and 56-m elevation for direct comparison with the tall tower observations. The namelist settings are available in the supporting information.

2.3.1. Gas-Phase Chemical and Aerosol Mechanisms

The gas-phase mechanism applied is the Regional Acid Deposition Model, version 2 (RADM2; Stockwell et al., 1990), which contains 59 chemical species and 157 gas phase reactions, of which 21 are photolytic. The aerosol modules include the inorganic fraction of the Modal Aerosol Dynamics Model for Europe (MADE) and the Second Organic Aerosol Model (SORGAM) for the carbonaceous fraction (Ackermann et al., 1998; Schell et al., 2001). Three log-normally distributed modes were applied for the simulation of particle size distribution in the MADE/SORGAM mechanisms, including the Aitken mode (<0.1-μm diameter), accumulation mode (0.1–2 μm), and coarse mode (>2 μm).

The chemical boundary conditions applied idealized profiles, which were embedded in the WRF-Chem model, and then by running the model for 1 week prior to each 1-month simulation, the simulated chemical fields at the end of this 7-day WRF-Chem spin up were applied as the background values for our simulations (Chu et al., 2018; Tuccella et al., 2012). Initial and boundary conditions for relevant meteorological fields were based on reanalysis data from the National Centers for Environmental Prediction with horizontal and temporal resolution of 1° and 6 hr, respectively. The physical configurations are summarized in Table S1 in the supporting information.

In WRF-Chem, the dry deposition (F_d) of NH_3 is simulated following the parameterization of Wesely (1989),

$$F_d = C_{NH_3} \times V_d \tag{1}$$

where C_{NH3} is the NH_3 mixing ratio at the first grid height and V_d represents NH_3 dry deposition velocity calculated as

$$V_d = 1/(r_a + r_b + r_c) \tag{2}$$

where r_a, r_b, and r_c represent the aerodynamic, quasi-laminar boundary layer, and canopy resistance terms, respectively. We note here that the WRF-Chem model framework does not yet include a dynamic bidirectional representation of the NH_3 fluxes. The potential limitations and uncertainties associated with this simplification are discussed further below.

2.3.2. Anthropogenic Emissions

Three different anthropogenic inventories were used in this study: EDGAR HTAP v2 (hereafter EDGAR) for global emissions, as well as NEI 2011 and NEI 2017 (derived based on NEI 2011 and hereafter defined as derived NEI 2017) for North American emissions (EPA, see details in section 2.3.3). EDGAR provides monthly emissions, while NEI provides an annual emission estimate. It is well known that NH_3 emissions exhibit strong seasonal variations and are generally highest in spring/summer; however, the EDGAR NH_3 emission rates for November are close to the annual average (scaling factor: 94.1%). Therefore, we applied the NEI annual emissions for the simulation of NH_3 in November. For other months, we did not apply monthly scaling factors on NH_3 emissions given that large biases were previously reported (Paulot et al., 2014) and we also found that the monthly scaling factors for EDGAR HTAP v2 and v4.3.1 products showed poor agreement for each month and differed by as much as a factor of 3 during the spring and summer (Figure S1 in the supporting information). Further, based on our sensitivity tests (Table S2), the simulated ground-level NH_3 mixing ratios and the dry deposition changed almost linearly with changes in NH_3 emission. For these reasons, we also applied these monthly scaling factors (derived from EDGAR HTAP v2, which looks more reasonable than v4.3.1; Figure S1) offline to calibrate NH_3 mixing ratio and dry deposition for comparisons, as discussed in section 3.5.

For perspective, within a 100-km radius of the tall tower, agricultural NH_3 emissions (fertilizer and livestock) accounted for 92% (2.30 nmol $\cdot$ $m^{-2} \cdot s^{-1}$) of annual total emissions based on the EDGAR dataset, with the remaining 8% attributed to energy, industry, residential, and transport categories. The annually averaged NH_3 emission for the U.S. Corn Belt was 1.53 nmol $\cdot$ $m^{-2} \cdot s^{-1}$. Hotspot emissions of 5.00 nmol $\cdot$ $m^{-2} \cdot s^{-1}$ were associated with intensive livestock operations near the northern border of Iowa (Figures 2a–2c).

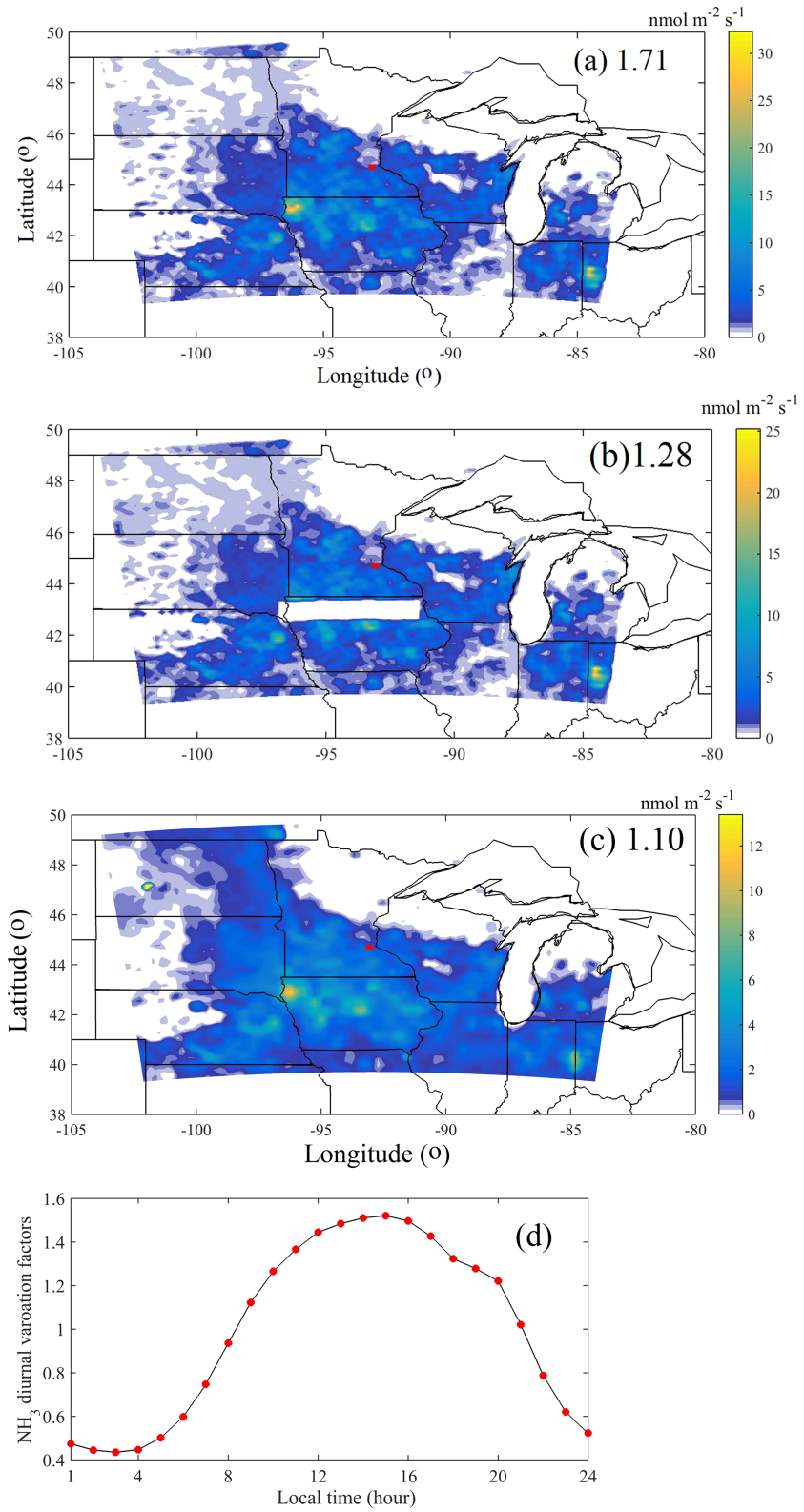

Figure 2. (a) National Emission Inventory (NEI) 2011 NH_3 emissions for Case 1, (b) North Iowa hotspot removed for Case 4, (c) Emission Database for Global Atmospheric Research (EDGAR) emissions for Case 6, and (d) diurnal variations factors of NH_3 in NEI 2011. Note that the numbers indicate domain-averaged NH_3 emissions.

According to the USDA 2018 report on agricultural products, 36% of U.S. hogs are raised in Iowa. The NEI 2011 emission inventory indicated that fertilizer and livestock accounted for 41.2% and 58.8% of the total agricultural emissions for Minnesota. In Iowa, these emissions accounted for 26.6% and 73.3%, respectively.

NEI 2011 is the most recent inventory available for conducting these WRF-Chem experiments. We applied annual scaling factors (Table S3, https://www.epa.gov/air-emissions-inventories) from EPA for both Minnesota and the United States in order to derive NEI 2017 pollutant emissions (including NH_3, CO, NO, NO_2, SO_2, $PM_{2.5}$, and PM_{10}) for the year of our analysis (2017) based on the NEI 2011 inventory. We note here that the EPA assumed pollution emissions that were constant from 2014 to 2017 given the lack of available data at the state scale. The scaling factor for 2014 was thus applied for the NEI 2017 emissions for domain 3. Based on the EPA annual NH_3 emission trends (not including biomass burning) for Minnesota and the United States, NH_3 emissions have decreased from about 2.06×10^5 tons in 2011 to 1.39×10^5 tons (32.5% decrease) in 2014 for Minnesota and decreased from 4.24×10^5 tons to 3.56×10^5 tons (15.5% decrease) for the United States from 2011 to 2017.

2.3.3. Case Studies and Model Experiments

We used the following case studies to gain new insights into regional NH_3 emissions, source transport, and dry deposition behavior. The simulation periods included November for both 2017 and 2018 and four example months in 2017. Cases 1–6 are focused on relatively high NH_3 emission episodes in November 2017 and Case 7 examined very low emissions during November 2018 using parallel model experiments. Finally, in Case 8, we extended the analyses to four example months in 2017 representing the four seasons to evaluate annual NH_3 emissions and dry deposition. The most recent state-of-the-art emission inventory is NEI 2011. Here, we use NEI 2011 as the baseline for comparisons outlined in the case studies below. Further, we derived the NEI 2017 emissions with the assumption that there are no spatial variations in emission trends observed from 2011 through 2017.

Case 1 involves simulations for November 2017, which is based on emissions prescribed using NEI 2011 and is used here as a first try and baseline simulation (Figure 2a). This case aims to simulate the hourly NH_3 mixing ratios and dry deposition and is compared with the tall tower observations to see whether the high NH_3 episodes can be captured by the WRF-Chem model and the NEI 2011 NH_3 emission inventory.

Case 2 focuses on the same period (November 2017) and uses temporally constant (without hourly variations) NH_3 2011 emissions with all other conditions the same as for Case 1. When compared with the tall tower NH_3 mixing ratio observations, Case 2 can be used to quantify the meteorological effect on NH_3 emissions and mixing ratios.

Case 3 applies the derived NEI 2017 inventory and compared the results with Case 1 to examine if the NH_3 emission trends provide a more accurate simulation than NEI 2011. This case represents a best estimate of 2017 emissions.

Case 4 uses the same emissions as prescribed for Case 3. However, the NH_3 emission hotspots in northern Iowa (42.5–43.5°N, 91–96.5°W, around 450 km^2) were zeroed out (Figure 2b) to help quantify how these hotspots in the U.S. Corn Belt impact regional NH_3 distribution and transport. Specifically, we used Case 4 to examine how much these NH_3 hotspots contributed to the tall tower observations in Minnesota.

Case 5 applies zero NH_3 emissions in both domains 2 and 3 for November 2017 (other pollution emissions are the same as for Case 1), while the NEI 2017 inventory is used for domain 1. This case is a zero local emission study. Case 5 was used to quantify the NH_3 mixing ratio and dry deposition associated with long-range atmospheric transport by comparing the results with Case 3.

Case 6 uses NH_3 emissions from the EDGAR inventory (other pollution emissions are the same as for Case 1) and then compared the results with the NEI 2011 simulations and observations to examine which inventory best simulated the high emission event observed in November 2017 (Figure 2c).

Case 7 examines differences in observations and simulations for November 2018 (lower NH_3 mixing ratio observations) and November 2017 (higher NH_3 mixing ratios) using all three inventories. Case 7 provides an opportunity to better understand the factors contributing to high NH_3 emissions and our ability to simulate them. It provides a good opportunity to evaluate the temperature sensitivity of NH_3 emissions.

Case 8 aims to quantify the annual dry deposition to managed and natural ecosystems and to evaluate the atmospheric transport processes on the observed seasonal NH_3 mixing ratio variations. Four months are simulated (using derived NEI 2017 emissions) in 2017 to represent seasonal variation (spring: May, summer: August, autumn: November, and winter: February); see details in sections 3.4 and 3.5.

3. Results and Discussions

3.1. Spatial Distribution of NH_3 Emissions

The spatial distribution of NH_3 emissions from NEI 2011 and EDGAR inventories is shown in Figures 2a and 2c (and Table 2). Ammonia emissions from NEI 2011 and derived NEI 2017 were larger than from EDGAR, implying that a national inventory and a global inventory are unlikely to make use of the same level of details of emission information. Based on the EDGAR inventory, agricultural emissions play a dominant role in the regional NH_3 balance, accounting for 97% of total NH_3 emissions in domain 3. This value is close to the NEI 2011 value (i.e., 95%). Diurnal variation factors for NH_3 (scaled to the daily average; Figure 2d) were derived from the default WRF-Chem emission generator for different source categories. According to the EDGAR inventory, the mean emission rate from the Northern Iowa hotspot is 3.3 times that of the U.S. Corn Belt average and 2.9 times that of our study domain 3. This hotspot is related to intensive livestock production where 22.6 million hogs were raised in Iowa in 2018, representing 35.9% of the national hog production.

3.2. Evaluation of Simulated Meteorological Fields and $PM_{2.5}$

Comparisons between observed and simulated T_2, RH, WD, and WS are displayed in Figure S2 and Table S4. The statistical metrics (RMSE: root-mean-square error, MB: mean bias, and R^2: correlation coefficient) indicate reasonably good performance for these selected variables. WS was slightly overestimated, perhaps because of discrepancies in surface roughness between the WRF-Chem grid cell (i.e., 5-km resolution) and the field scale (i.e., less than 100-m resolution) observations where roughness is consistent and well defined. Overall, these comparisons did not reveal large or persistent biases that would be expected to significantly compromise the model-measurement analyses for NH_3.

The PBL height is a critical factor controlling scalar concentration variations. Hu et al. (2018) and Fu et al. (2017) conducted atmospheric inverse analyses for this same study domain and tall tower site for CO_2 and N_2O budgets, respectively. Their results indicated relatively good performance in simulating PBL height using the WRF model with the same boundary layer scheme (Yonsei University [YSU] scheme), as applied in our WRF-Chem simulations. Figure S3 shows that the WRF-Chem model generally reproduces the diurnal variations of PBL height and simulated a lower PBL height than NARR ($R^2 = 0.52$ for 2017 and 0.53 for 2018, $p < 0.001$; RMSE = 427 m for 2017 and 414 m for 2018). Here we note that the NARR PBL height was unrealistic for a number of days (e.g., days 11–14 and days 25–27, November 2018), with PBL heights greater than 1,000 m during the nighttime. Based on the observations for winter 2009 at a nearby observation site, the WRF-Chem simulations show close agreement with the observations at 6:00 and 18:00, where the observations were 217 ± 42 m (mean ± *SD*) at 6:00, and 337 ± 36 m at 18:00. The WRF-Chem model showed lower bias than NARR (Figure S3c).

Variations in mass concentrations of $PM_{2.5}$ were well captured by WRF-Chem (Figure 3 for Cases 3 and 6). Daily averages for $NH4^+$, NO_3^-, and SO_4^{2-} particles are also displayed in Figure S4. When derived NEI 2017 was specified as the emission source, the primary $PM_{2.5}$ emissions were 76% of the EDGAR case (Table S3) and simulated NH_4^+ particles were 0.11 and 0.10 μg/m^3 for NEI 2017 and EDGAR respectively, indicating a relatively small role in secondary $PM_{2.5}$ formation (Figure 3 for $PM_{2.5}$). The simulated $PM_{2.5}$ results were between Cases 3 and 5 (without NH_3 emissions within domains 2 and 3) and showed that the domain 3 averaged ground-level $PM_{2.5}$ decreased by only 0.27 μg/m^3 (<5% of total 5.55 μg/m^3) even without any NH_3 emissions within domains 2 and 3. This indicates that agricultural NH_3 emissions play a relatively minor role in total particle formation within this domain.

As shown in Figure 3, both emission cases performed well in simulating the daily variations of $PM_{2.5}$ for the five sites. Here, the EDGAR emission case resulted in an RMSE of 4.37, 5.08, 6.31, 3.54, and 3.63 μg/m^3 for Apple Valley, Ben Franklin School, Harding High School, Talahi School, and Michael Elementary School sites, respectively. The RMSEs for Case 3 (the derived NEI 2017 emission case) were slightly lower at 4.10,

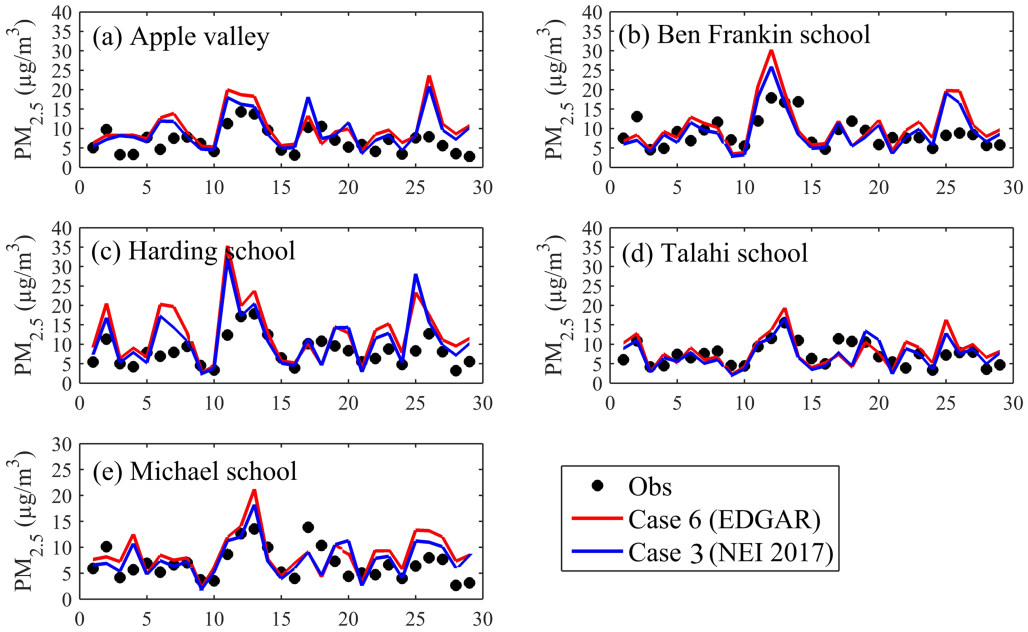

Figure 3. (a–e) Comparison of daily averaged particulate matter 2.5 between WRF-Chem simulations and five Environmental Protection Agency (EPA) observation sites for November 2017and (f) combined data for all site observations and simulations. Note that National Emission Inventory (NEI) 2011 case (Case 1) was not shown because it has the same emissions (exclude NH_3) and almost identical results as Emission Database for Global Atmospheric Research (EDGAR) case.

4.58, 5.90, 3.30, and 3.28 μg/m^3, respectively. The observations and simulations showed a peak between days 10 and 15 for November 2017. The simulated values were slightly overestimated at Ben Franklin School and Harding High School sites. In general, both the observed and modeled low $PM_{2.5}$ mass concentrations are attributed to low primary $PM_{2.5}$ emissions and relatively low NOx and SO_2 emissions within this agricultural dominated region.

The 1:1 plot (Figure 3f) summarizes the model $PM_{2.5}$ performance for all five sites and for both emission cases including NEI 2017 and EDGAR. The ensemble five-site average values were 8.92 and 9.96 μg/m^3 for NEI 2017 and EDGAR cases, respectively, and were 17.3% and 31.1% higher than the average value of the observations (7.60 μg/m^3). The overall performance was very good for the derived NEI 2017 case, which slightly overpredicted $PM_{2.5}$ (MB = 1.32 μg/m^3, $R = 0.58$ for both $p < 0.001$). The difference between the EDGAR versus derived NEI 2017 simulated $PM_{2.5}$ was mainly attributed to the primary $PM_{2.5}$ emissions, where the primary $PM_{2.5}$ emission for the derived NEI 2017 case was 76% of EDGAR. Further, the model simulations indicated that the secondary particles from NH_3, NO_x, and SO_2 emissions made a minor contribution (Figure S4). When emissions were specified using the derived NEI 2017 emissions, the WRF-Chem simulated $PM_{2.5}$ was closer to the 1:1 line in Figure 3f. We note here that the EPA assumed that state-level pollution emissions were constant from 2014 to 2017 due to a lack of available data. We therefore hypothesize that reduced primary $PM_{2.5}$ emission for the years 2014 to 2017 can help to explain the model overestimate of the observations.

3.3. Simulations of November NH_3 Mixing Ratios and Dry Deposition Fluxes

3.3.1. Spatial Distribution of NH_3 Mixing Ratios

The spatial distribution of simulated NH_3 mixing ratios is displayed in Figures 4a and 4b. Because there was high spatial correlation, with respect to the distribution, between simulations using NEI 2011, derived NEI 2017 and EDGAR, we have shown only results for Case 3 of derived NEI 2017. Monthly averages from 7 AMoN sites and the KCMP tower are also shown and were found to be highly correlated with the simulated NH_3 mixing ratios. Intensive livestock production in northern Iowa is an NH_3 hotspot within our study

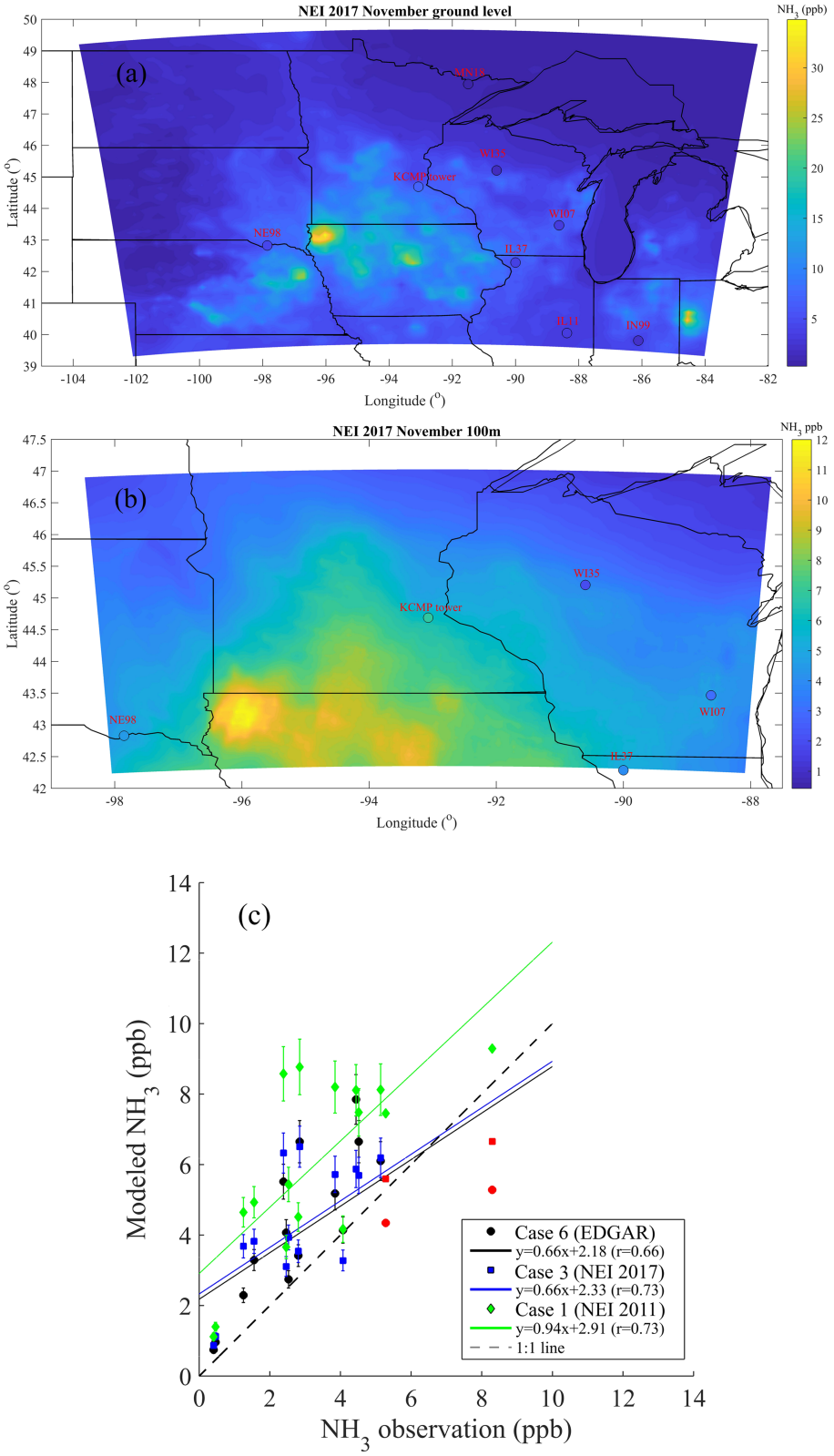

Figure 4. (a) Spatial distribution of simulated NH_3 mixing ratios at ground-level for domain 2: note that Ammonia Monitoring Network (AMoN) site observations are at ground-level; (b) 100-m height for domain 3 for November 2017, NH_3 observations of seven AMoN sites, and KCMP tall tower are also shown. (c) Comparisons between model results with AMoN and tall tower observations (in red colors), biweekly results are shown, and the error bars indicated 9% relative error.

domain. The simulated NH_3 mixing ratios at this hotspot exceeded 30 ppb at the ground-level. Further, the simulations also show that agricultural lands in southern Minnesota are associated with high NH_3 mixing ratios.

The simulated NH_3 mixing ratios at the 100-m height above these agricultural hotspots reveal that averaged mixing ratios can exceed 10 ppb. These simulations for the 100-m height also illustrate the effect of atmospheric transport from northern Iowa to Minnesota. The difference of NH_3 mixing ratios (Case 3 versus Case 4—i.e., simulations with and without emissions from the northern Iowa hotspots) is shown in Figure S5. It reveals that northern Iowa hotspots can have a strong influence on regional NH_3 mixing ratio distributions and also at the KCMP tower site. The results indicate that these emissions contributed to a mean 1.07 ppb enhancement at 100-m height during November, which is 17.6% of the simulated NH_3 mixing ratios and indicates a significant contribution via long-distance transport. Considering the average distance (400 km) between KCMP and the Iowa hotspot and a simulated November WS of 5.0 m/s at the 100-m height, the average transport time was about 23 hr.

The large vertical gradient in NH_3 mixing ratios between ground-level and the 100-m height can reflect variations in emissions, deposition, or atmospheric chemical reactions related to gas-particle phase partitioning. As noted above, the simulated ammonium particle concentration was relatively small (<0.15 $\mu g/m^3$ equivalent to <0.18 ppb gaseous NH_3). This suggests that these vertical NH_3 mixing ratio gradients are driven primarily by emissions and deposition. The NH_3 mixing ratio profiles at our tall tower site are shown in Figure S6. Each case demonstrates that the profile decreases logarithmically with increasing height. To better understand the vertical distribution of NH_3 mixing ratios, we compared the model simulations with the tall tower observations from the 100- and 56-m heights. Here, the average NH_3 mixing ratio observations were 6.64 and 6.76 ppb for the 100- and 56-m levels in November 2017, respectively. The observations thus showed a mean NH_3 mixing ratio gradient of −0.27 ppb/100 m when assuming a linear fit as a function of height extending to 100 m. The simulated gradients for the tall tower location ranged from −0.21 to −0.84 ppb/100 m and were in good agreement with the observations (data shown in Figure S6). For most of the simulation cases and observation periods, the negative gradient between 100 and 56 m indicated that the study domain acted as a net NH_3 source.

It is interesting to note in Case 5 (zero local emissions scenario for hotspots in domains 2 and 3) that the modeled NH_3 mixing ratios exhibited a positive gradient (i.e., increasing with increasing height) below 300–500 m, which is the opposite direction of the other cases. Here, the NH_3 mixing ratio peaked at ~400 m and decreased both above and below this height. This indicates that this height acts as a transition layer where downward and long-range-transport NH_3 from outer domain was balanced. Similar results have been observed near the Colorado Front Range, USA (Li et al., 2017; Tevlin et al., 2017), where some individual profile observations have shown a decreasing NH_3 gradient below 10 m and an increase above this height when the land acts as a strong NH_3 sink. Further, aircraft NH_3 observations near coastal Virginia and Maryland, USA, reveal vertical gradients (~0.3 ppb per 1 km) with NH_3 mixing ratios increasing with increasing height above the surface, indicating that the surface was acting as a net NH_3 sink (Lebel et al., 1985).

3.3.2. Comparisons Between Simulated and Observed Hourly NH_3 Mixing Ratios

Simulated hourly NH_3 mixing ratios for November 2017, using three different NH_3 emission inventories, were compared with the 100-m NH_3 observations in Figure 5a. The monthly averages were 6.65, 8.44, 4.82, and 6.11 ppb for the observations, NEI 2011 (Case 1), EDGAR (Case 6), and derived NEI 2017 (Case 3), respectively. The RMSE among NEI 2011, EDGAR and derived NEI 2017 were 6.09, 5.12, and 5.37 ppb, respectively. The simulated NH_3 mixing ratios using NEI 2011 emissions were biased high before 12 November and on 20 November. Simulations based on derived NEI 2017 and EDGAR emissions performed better during the same period, and after 13 November. The simulations based on EDGAR emissions were slightly lower than the tall tower observations. In general, derived NEI 2017 gave the overall best fit to the observations of November 2017. As shown in Figure 5a, the observations reveal nine high (i.e., greater than 10 ppb) NH_3 mixing ratio episodes during this study period. These episodes were consistent in having southerly wind flow and increasing air temperature (Figure 5c). Observed NH_3 mixing ratios reached 35 ppb on 15 November with three other episodes occurring on 20, 24, and 28 November that exceeded 20 ppb. The model results showed high consistency with the NH_3 observations and performed well in reproducing all

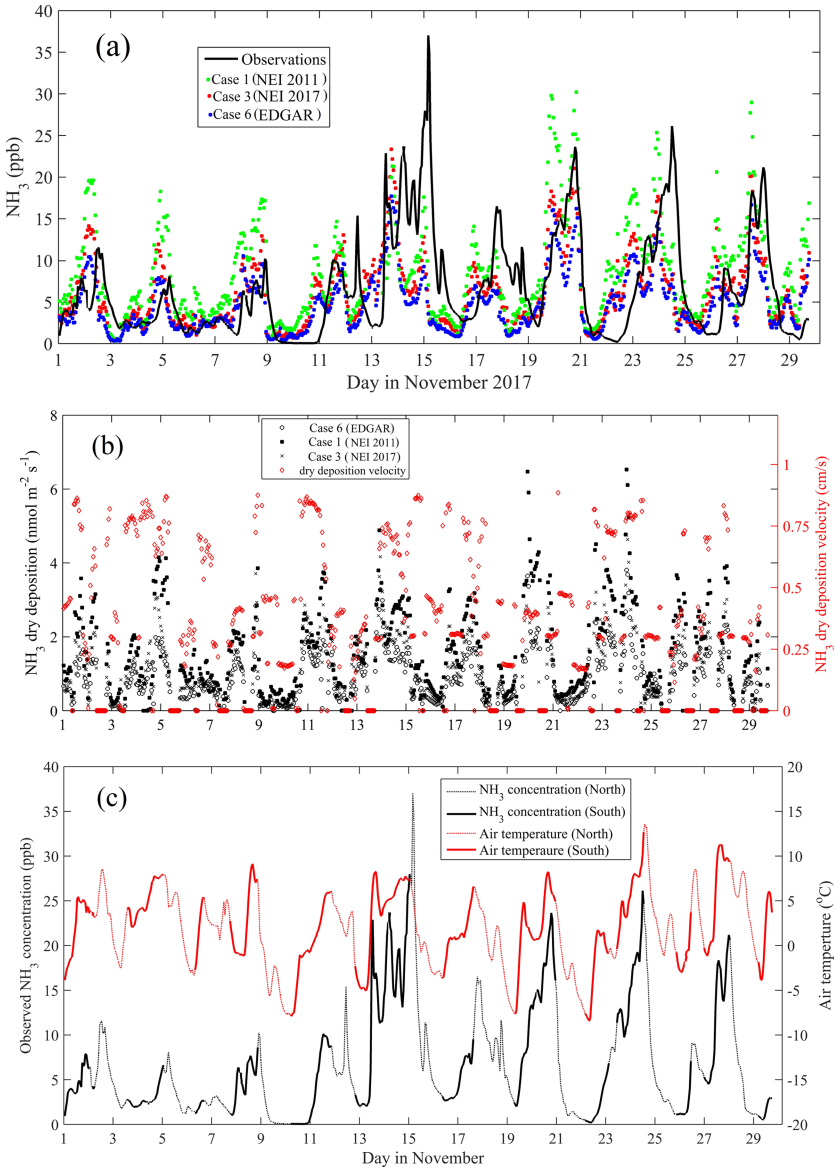

Figure 5. (a) Comparisons of NH_3 mixing ratios between observations and simulations using different NH_3 emissions, (b) simulated dry deposition flux and velocity for NH_3, and (c) the relationship between wind direction, air temperature and NH_3 observations.

nine high NH_3 emission episodes observed in November 2017. A recent study in Ireland defined five different health risk categories associated with varying NH_3 concentrations. The most serious health risk is associated with NH_3 mixing ratios in excess of 4 $\mu g/m^3$ (~5.3 ppb; Kelleghan et al., 2019). Thus, ground-level NH_3 mixing ratios for our domain 3 frequently (336 hr, 48% of this month) exceeded this threshold in November 2017 when using the derived NEI 2017 inventory.

Here, we examine the key drivers that can influence these high NH_3 episodes. As shown earlier, particulate NH_4^+ makes up only a minor fraction of the NH_x budget and thus does not explain the episodes. The synoptic weather patterns can control such high episodes with southerly air flow transporting emissions from key source areas. Further, the model simulation and observational results described above, occasionally exhibiting high or low biases, indicate that NH_3 emissions cannot be explained with only activity data and constant EFs. For instance, the reported Q_{10} of NH_3 emissions can vary from 1.25 to 4.6 (Riddick et al., 2016; Sutton et al., 2013; Zhang et al., 2017) indicating relatively strong sensitivity to air temperature. During our study

period, NH_3 EFs varied from 1.56 to 21 for air temperatures ranging from 12 to 33°C. Therefore, some of the model disagreement describe in Figure 5a is partially attributed to the variations in air temperature effect on NH_3 emissions that are not explicitly considered by these default NH_3 emission inventories.

In November 2018, NH_3 mixing ratios observed at the tall tower were substantially lower compared to November 2017. These observations and differences in weather and climate between years provide a unique opportunity to examine the fidelity of the WRF-Chem model simulations and the reasons for high NH_3 episodes. In these simulations the emissions are specified using the same inventories applied to November 2017. However, differences in meteorological conditions (i.e., transport, boundary layer height, and temperature) varied between these years. We compared the simulated PBL heights between these two periods with 416 m for 2017 and 448 m for 2018, indicating a minor role in the simulated NH_3 difference. The observed November T_2 in 2017 was 3.1°C higher than 2018, which was in relatively good agreement with modeled difference of 2.32°C, indicating that higher air temperature in November 2017 enhanced NH_3 emissions. The observed frequency of southerly wind flow decreased from 37.1% in November 2017 to 27.6% in November 2018. Further, the actual amounts of synthetic and organic nitrogen fertilizer applied within the study domain are expected to be relatively consistent based on recent fertilizer trends (Griffis et al., 2019). In this way, the model simulations can be used to help isolate how different factors influence these observations.

For November 2018, the observed monthly average NH_3 mixing ratio was 3.75 ppb. The simulated monthly average mixing ratios were 6.53, 3.49, and 4.46 ppb based on the NEI 2011 (Case 1), EDGAR (Case 6), and derived NEI 2017 (Case 3) emission inventories, respectively (Figure 6). The RMSE between NEI 2011, EDGAR, derived NEI 2017, and the observations were 4.32, 2.80, and 3.22 ppb, respectively. The model results based on NEI 2011 were consistently biased high. The results based on derived NEI 2017 and EDGAR emission inventories showed better agreement with the observations over the entire month. Further, the simulated NH_3 mixing ratios in November 2018 also showed high NH_3 episodes that exceeded 20 ppb. These simulated episodes, however, were not consistent with the tower observations. This discrepancy between November 2017 and November 2018 suggests that the temperature sensitivity of NH_3 emissions is strong (not captured by the model) on NH_3 emissions. The average NH_3 observations in November 2017 were 1.77 times when compared with November 2018. The ratios (simulated NH_3 mixing ratios) of NEI 2011 (Case 1), EDGAR (Case 6), and derived NEI 2017 (Case 3) between November 2017 and 2018 were 1.29, 1.38, and 1.37, respectively. Because the WRF-Chem model applied the same emissions for these 2 years, these ratios of 1.29 to 1.38 can be used to help isolate the effect of atmospheric transport on NH_3 mixing ratios. For example, WD differences between these years, in relation to the source distribution, is one key factor causing the large difference in mixing ratios between the two years. Note that NH_3 mixing ratio observation differences between these two years are primarily attributed to both atmospheric transport factors and changes in actual NH_3 emissions. Further, the results of 1.37 (1.77/1.29) to 1.28 (1.77/1.38) can be attributed to emission differences between November 2017 and November 2018.

3.3.3. Temperature Effect on NH_3 Mixing Ratio and Emissions

The combination between large air temperature differences with higher concentrations (after accounting for other meteorological effects) between November 2017 and 2018 provides evidence that temperature can have a substantial effect on the NH_3 EFs. Based on previous field studies, the observed EFs are considered zero when the air temperature is below 0°C (Sutton et al., 2013; Xiuming Zhang et al., 2017), Here, we attempt to quantity the sensitivity of NH_3 emissions based on simulated NH_3 mixing ratios and average domain 3 simulated air temperatures at the 2-m level. The average T_2 were 1.49°C in November 2017 and 0.76°C in November 2018. We also calculated the cumulative temperature, when air temperatures exceeding the freezing temperature, in November for these two years, and found that the cumulative T_{2m} was 1625°C for November 2017 and 1018°C for November 2018. The cumulative T_{2m} in 2017 was 1.60 times than that of 2018. These results suggest that the higher temperatures in 2017 caused higher NH_3 EFs and emissions. The temperature effect (Q_{10}) will be further discussed below.

Case 2 used temporally constant NH_3 emissions, for November 2017, to help isolate the meteorological effects on NH_3 emissions. Both observations and the WRF-Chem model results revealed an exponential relationship between NH_3 mixing ratios and air temperature. The Case 2 results also reveal the exponential relationship between NH_3 mixing ratios and air temperatures (even though NH_3 emissions from the

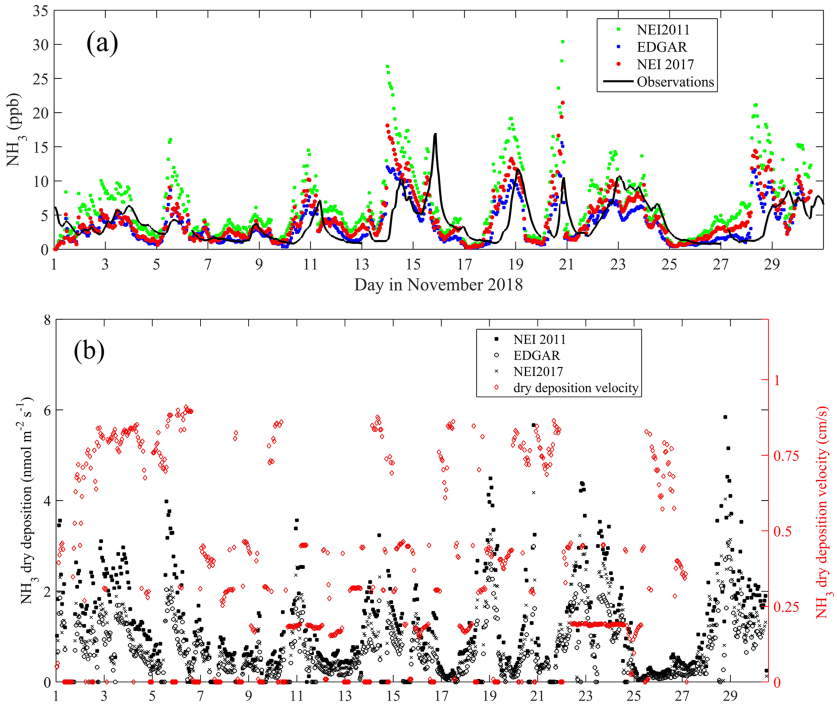

Figure 6. Simulations for November 2018 for (a) comparisons of NH_3 mixing ratios between observations and simulations using different NH_3 emissions) and (b) dry deposition flux and velocity for NH_3.

inventories are not temperature dependent), indicating that the observed and modeled exponential relationships were not solely caused by the sensitivity of NH_3 emissions to temperature but also by atmospheric transport processes such as a change of WD in relation to source distribution.

We fit an exponential relation to these data as shown in Figure 7a. There are three potential explanations for these relations. First, higher air temperature caused higher NH_3 emissions (biological sensitivity, excluding Case 2). Second, higher air temperatures were correlated with synoptic weather patterns and southerly air flow where there are known NH_3 hotspots (transport sensitivity; i.e., there is correlation between air temperature and WD and source area). Third, higher air temperature favors NH_4NO_3 particle partitioning to gaseous NH_3. However, as discussed above, we believe that this last factor is negligible for this region. Based on the regression analyses of the tall tower observations, we found that NH_3 mixing ratios increased from about 4 to 19 ppb (Q_{10} = 4.8, including both biological sensitivity and transport sensitivity) when air temperature increased from 0 to 10°C. Case 2 showed that NH_3 increased from about 7 to 13 ppb, indicating a Q_{10} of 1.9 (i.e., this only represents the transport sensitivity). The relative changes from 1.9 to 4.8 times can only reflect the biological sensitivity on NH_3 emissions that was mainly caused by air temperature; we therefore interpret the ratio 2.5 between the two as the temperature sensitivity of NH_3 emissions.

Dynamic reemission of NH_3 is not accounted for in the WRF-Chem model, which may bring some potential biases and uncertainties in the temperature-dependent simulations. These uncertainties are likely to be within the overall uncertainties of the simulated gross NH_3 emissions, because the EFs of agricultural NH_3 emissions are based on field experiments, which also contain the reemission of deposited NH_3. Here, the simulated NH_3 mixing ratios from April to September are in very good agreement with the tall tower observations. Most of the scatters in these plots are close to the 1:1 line, and their histograms show very similar distributions. Some of the large departures might be related to the fact that we do not simulate bidirectional NH_3 flux or they could result from transport errors in the model simulations. Further, we also note that there is relatively good agreement between our estimate of NEE and that observed based on the tall tower flux-gradient observations (Griffis et al., 2019).

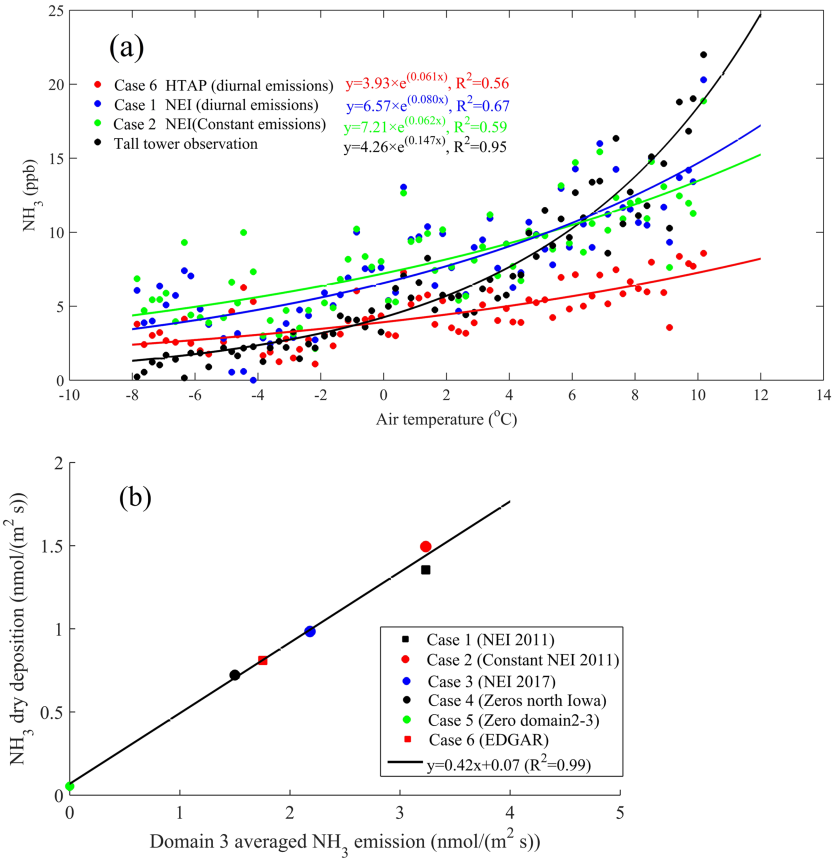

Figure 7. (a) Exponential relationship between 2 m air temperature and NH_3 mixing ratios for different case studies and (b) the linear relationship between NH_3 emissions and dry deposition flux in six cases for November 2017.

These results for Q_{10} agree reasonably well with previous studies (Riddick et al., 2016; Sutton et al., 2013; Zhang et al., 2017). Sutton et al. (2013) used a land-atmosphere model that included a bidirectional NH_3 flux scheme. Their model incorporated the effects of temperature and moisture on NH_3 emissions. They showed that NH_3 emissions increased by 42% (28–67%) when the model temperature increased by 5°C, indicating a Q_{10} of 2.0 (1.6–2.8) in their model. Zhang et al. (2017) applied Q_{10} values of 1.25–2.50 for different NH_3 sources and used a value of 2.0 for all fertilizer applications. These Q_{10} values are similar to those derived from our tall tower NH_3 observations and WRF-Chem modeling.

3.3.4. Interpreting the Relationship Between NH_3 Emissions and Dry Deposition Flux

We examined the relation between NH_3 emissions and deposition for the case studies described above. Figure 7b illustrates that there is a strong linear relationship between NH_3 emissions and the dry deposition flux for the six different emission scenarios of our study. This relation appears to be robust and holds for the two extreme experimental cases of zero flux for domains 2 and 3, and zero flux for the hotspots near northern Iowa, where the NH_3 distribution can deviate substantially from the other four test cases. The domain-averaged dry deposition flux can be estimated using the regression equation $y = 0.42x + 0.07$ ($R^2 = 0.99$, $p < 0.001$), where x and y represent NH_3 emissions and dry deposition flux (nmol $\cdot$ m^{-2} $\cdot$ s^{-1}), respectively. The slope is unitless and represents the domain-averaged dry deposition characteristics (Figure S7), which are mainly dominated by land surface characteristics and meteorological fields (Wesely, 1989; Wu et al., 2011). We further calculated domain 3 averaged dry deposition velocities for these six cases, and the result was 0.44 ± 0.01 cm/s (ave ± *SD*), with its value almost the same as the slope. This indicates that 42% of emissions within this domain were deposited within the region and that the other 58% was transported out of the region. The intercept 0.07 is close to the dry deposition of Case 5 (0.06 nmol $\cdot$ m^{-2} $\cdot$ s^{-1}) and can be interpreted as the dry deposition without regional emissions, resulting only from the long-distance transport

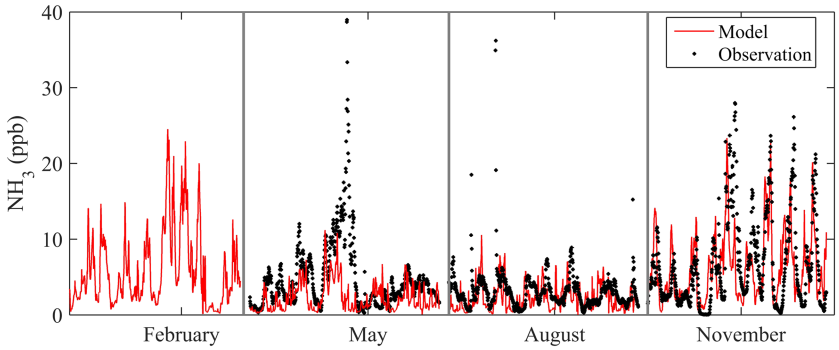

Figure 8. Time series of observed and modeled hourly NH_3 mixing ratios of Case 8 for each typical month.

from the outermost domain. Using this relation, we estimated NH_3 NEE to be 58% of gross emissions for November 2017. These results are consistent with our previous flux-gradient estimates, which concluded that dry deposition accounted for about 30–40% of gross emissions, with the remaining 60–70% for NH_3 NEE (Griffis et al., 2019).

3.4. Annual NH_3 Mixing Ratio Comparisons for 2017

To provide an annual view of NH_3 mixing ratios and NH_3 NEE, we extended our analyses from November to other months (February, May, August, and November) in 2017. The WRF-Chem NH_3 simulations, using the derived NEI 2017 emission inventory, were compared to the tall tower 100-m observations for each month. As shown in Figure 8, the model simulations generally capture the episodic and diurnal variations of the observed NH_3 mixing ratios with RMSE (R^2) of 3.69 ppb (0.36), 2.22 ppb (0.13), and 5.37 ppb (0.49) for May, August, and November 2017, respectively. The WRF-Chem model performed well in capturing the relatively low NH_3 observations in August and the higher NH_3 values in November 2017. The observed high NH_3 episodes in the middle of May were not captured by WRF-Chem. These large emissions were likely driven by synthetic fertilizer application within the region, which is typical for this time period (Griffis et al., 2017). Here, the simulations underestimated the emissions during this period. Previous research has suggested that spring emissions were underestimated by emission inventories such as NEI (Butler et al., 2016; Paulot et al., 2014).

3.5. Net Ecosystem NH_3 Exchange

The study domain provides a unique opportunity to examine strong emission and deposition patterns associated with agricultural lands to the south and west, and forested lands to the northeast and southeast (Figure 1). Based on the tall tower measurement-model comparisons above, the model is able to represent the drivers of NH_3 for this region, which supports its use to examine broader-scale processes such as regional NH_3 NEE. To assess regional net NH_3 sinks/sources in our study domain, we calculated the modeled NH_3 NEE for different cases. Figure 9a shows that the NH_3 NEE for 2017 (Case 6) was highly correlated with land surface categories, with positive NH_3 NEE in agricultural lands and negative in natural ecosystems. In northern Minnesota and Wisconsin we see a distinct transition from net NH_3 source (over croplands to the south and west) to a net sink (over forested areas to the north and east) related to the change in land use (Figures 9a and 1b and 1c). This spatial distribution of NH_3 NEE is mainly controlled by the NH_3 emission and mixing ratio distributions rather than V_d, where V_d has much smaller spatial variations (Figure S5).

The WRF-Chem model framework does not yet have a bidirectional NH_3 flux scheme, which may result in some limitations and uncertainties when simulating the NH_3 mixing ratios. A few other models have taken bidirectional exchange into account (Bash et al., 2013; Cooter et al., 2012; Pleim et al., 2013; Whaley et al., 2018). Previous work with the CMAQ model suggests that this will lead to a slight overestimation of NH_3 dry deposition (Lonsdale et al., 2017; Lv et al., 2019), and in some regions (e.g., boreal forests), other modeling platforms have suggested that bidirectional fluxes may locally have a controlling impact on atmospheric ammonia concentrations (Whaley et al., 2018). However, in agricultural regions, such as the U.S. Corn Belt, the reemission of stored NH_3 can be considered as a minor factor compared to the gross emissions (Griffis

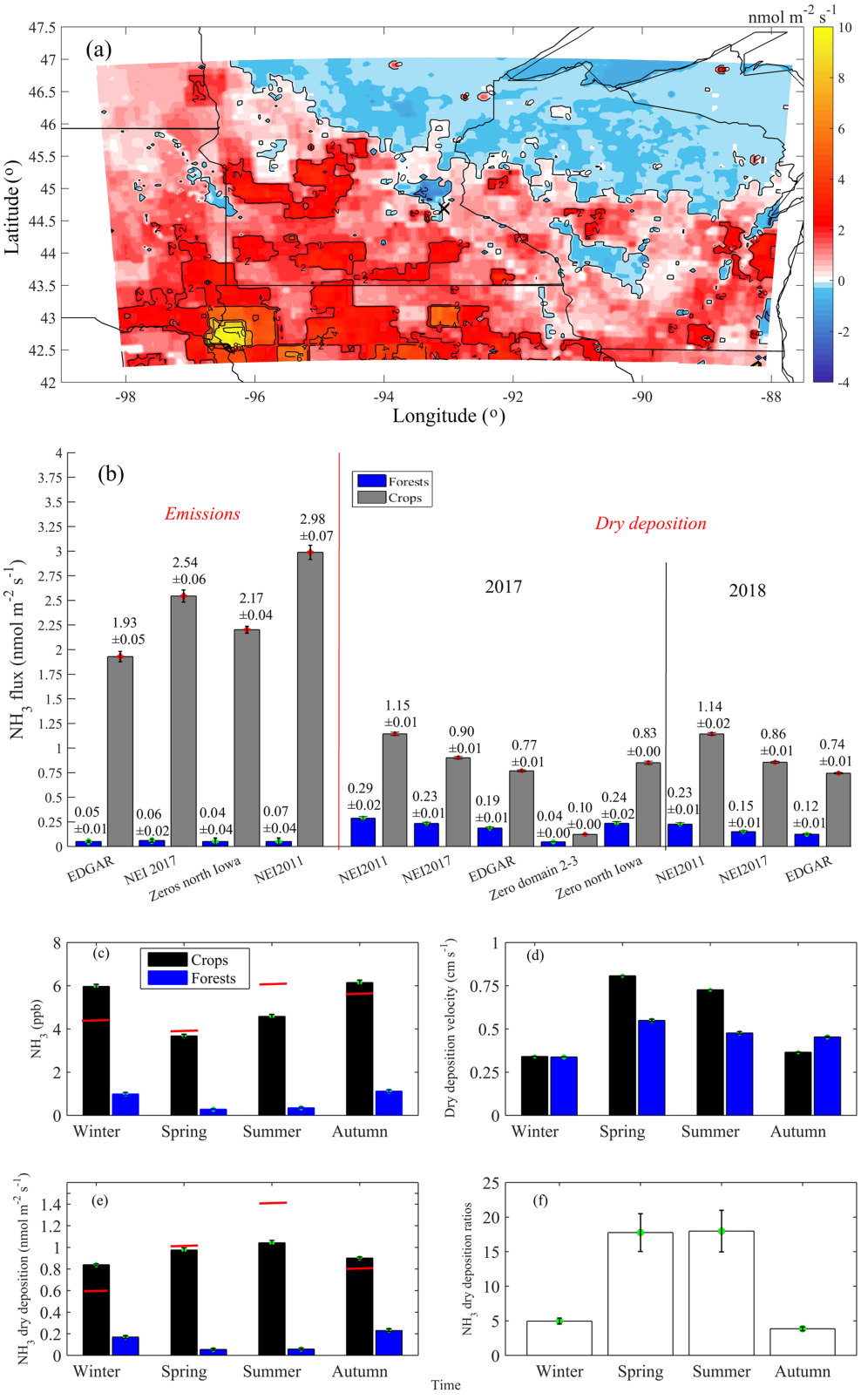

Figure 9. (a) Spatial distribution of the NH_3 net ecosystem exchange for Emission Database for Global Atmospheric Research (EDGAR) in November 2017, (b) NH_3 dry depositions for both forests and crops lands for different November (both 2017 and 2018) case studies, (c) seasonal variations of NH_3 mixing ratios, (d) dry deposition velocity, (e) dry deposition flux, and (f) its ratios.

Table 3
Mean Dry Deposition (nmol · m^{-2} · s^{-1}) in Different Land Use (Forests and Crops Are Shown), and NH_3 Mixing Ratio (ppb) Distributions for Forests Lands

Category	Land use	PFTs (%)	Case 1 201711 (NEI 2011)	Case 3 201711 (NEI 2017)	Case 4 201711 (zeros North Iowa)	Case 5 201711 (zeros Domain 2-3)	Case 6 201711 (EDGAR)	Case 7 201811 (NEI 2011)	Case 7 201811 (EDGAR)	Case 7 201811 (NEI 2017)
NH_3 dry deposition	Forests	>70	0.31	0.25	0.26	0.04	0.20	0.25	0.14	0.16
		>80	0.29	0.23	0.24	0.04	0.19	0.23	0.12	0.15
		>90	0.27	0.22	0.22	0.04	0.18	0.21	0.12	0.14
	Crops	>70	1.13	0.89	0.83	0.10	0.76	1.12	0.73	0.84
		>80	1.14	0.90	0.83	0.10	0.77	1.14	0.74	0.85
		>90	1.16	0.92	0.83	0.10	0.78	1.17	0.76	0.87
	Ratios	>70	3.63	3.54	3.20	2.43	3.76	4.56	5.40	5.25
		>80	4.00	3.87	3.48	2.61	4.11	5.07	6.03	5.80
		>90	4.36	4.18	3.73	2.72	4.46	5.53	6.57	6.21
NH_3 (ppb)	Forests	>70	1.51	1.20	1.17	0.21	0.96	1.18	0.66	0.79
		>80	1.41	1.12	1.09	0.20	0.90	1.10	0.61	0.73
		>90	1.30	1.04	1.00	0.20	0.84	1.01	0.57	0.67

Abbreviations: EDGAR: Emission Database for Global Atmospheric Research; NEI: National Emission Inventory.

et al., 2019; Sutton et al., 2013). We note that most of our observation station locations are in regions where cropland is the dominant agricultural land use type (see Figures 1c and 1d). Based on our own simulations for forested areas within our study area, we suggest that the reemission of deposition NH_3 can be safely ignored considering high use efficiency of nitrogen by plants and that the nitrate deposited in these forested areas can rapidly transport to streams and waters without being biologically transformed (Rose et al., 2015; Sebestyen et al., 2014). Significant atmospheric nitrate deposition has also been observed that dissolved in waters at the forest regions, with high spatial and temporal variations (Sebestyen et al., 2019).

We further examined NH_3 dry deposition rates, NH_3 NEE, mixing ratios, and V_d according to land use based on the November case studies described above (Table 3 and Figure 9b). The simulated NH_3 dry deposition varied between 0.19 to 0.29 nmol · m^{-2} · s^{-1} in forested lands (excluding the Case 5 background case) and 0.77 to 1.15 nmol · m^{-2} · s^{-1} on agricultural lands for the various case studies examined in November 2017 (excluding Cases 4 and 5). On average, NH_3 NEE over agricultural areas was upward (positive to the atmosphere) and accounted for 60.1–64.6% of gross NH_3 emissions. Conversely, the net exchange over forested areas was downward and was on average 2.8–3.1 times greater in magnitude than the gross emissions for these areas across the three inventories in November 2017. The results indicate that these natural ecosystems were important NH_3 sinks. Agricultural lands, however, were strong NH_3 sources with emissions 2.5 to 2.8 times the dry deposition rate. By comparing the November dry deposition in years 2017 and 2018, the deposition slightly increased in agricultural (3%) and largely increased in forested domains (46%) for the warmer November 2017 period (relative to November 2018). Thus, future warmer temperatures have potential to enhance agricultural N losses with dry deposition likely increasing in adjacent forested areas. These enhancements are likely to be of significant concern in the late fall and early winter months where warming temperatures overlap with substantial manure and synthetic nitrogen application to the landscape.

To quantify the transport effect of the northern Iowa NH_3 animal agriculture hotspot to nonagricultural ecosystems, we calculated the difference in forested NH_3 dry deposition between Case 4 (with no NH_3 emissions from northern Iowa) and Case 3 (the derived NEI 2017 case). The resulting difference was less than 1.6% for NH_3 dry deposition in the forested domain and indicated a relatively minor role of this NH_3 hotspot in long-distance transport to remote nonagricultural lands. Further, using Case 5 (zero flux for domains 2 and 3) and Case 3, we estimated that 83 ± 0.4% of the dry deposition to forested areas in our domain can be traced to agricultural emissions from within the U.S. Corn Belt in November 2017.

The simulated NH_3 NEE was within the range of values reported previously for a typical coniferous canopy with a NH_3 NEE flux between −64.7 and 14.1 nmol · m^{-2} · s^{-1} (Duyzer et al., 1992; Andersen et al., 1993, 1999; Pryor et al., 2001). For instance, our values were smaller than average observations for a coniferous forest (1.3 nmol · m^{-2} · s^{-1}) in southern Indiana (Pryor et al., 2001) and 0.54 nmol · m^{-2} · s^{-1} at a

Norway spruce forest in Denmark (Andersen et al., 1999). The main differences can be attributed to the atmospheric NH_3 abundance, as the Indiana and Denmark sites were in close proximity to high density agricultural lands (Table S5). For the Danish site, NH_3 emissions were approximately 7.0 nmol $\cdot$ $m^{-2} \cdot s^{-1}$ (data were not reported for the southern Indiana site) and provided an important source for downwind dry deposition. Their gross emissions were much higher than our tall tower estimation of 1.8–2.1 nmol $\cdot$ $m^{-2} \cdot s^{-1}$ (Griffis et al., 2019). For our study area, if we assume that forested lands in close proximity to agricultural lands have similar NH_3 mixing ratios as for agricultural areas, the modeled NH_3 dry deposition will be on the order of 1 nmol $\cdot$ $m^{-2} \cdot s^{-1}$.

Comparing our simulations with forested sites in previous studies, the observed annual average NH_3 mixing ratios were 0.54 $\pm$ 0.04, 0.54 $\pm$ 0.08, and 0.33 $\pm$ 0.11 ppb at three forest sites in Pennsylvania and New York State. The estimated dry deposition was 0.45 $\pm$ 0.07, 0.50 $\pm$ 0.09, and 0.32 $\pm$ 0.16 nmol $\cdot$ $m^{-2} \cdot s^{-1}$ for three different sites, which were also remote from major NH_3 emissions (Butler et al., 2015). These results are in good agreement with our simulations for forested sites that are also remote (i.e., >100 km) from agricultural NH_3 emissions.

We extended these analyses for different seasons of 2017 (Case 8). There is a substantial seasonal variation for NH_3 dry deposition velocity, NH_3 dry deposition flux, and atmospheric NH_3 mixing ratios (Figures 9c–9f). Further, we calculated the NH_3 NEE for agricultural lands in domain 2, which averaged 1.60 $\pm$ 0.06 nmol $\cdot$ $m^{-2} \cdot s^{-1}$. This value is consistent with our tall tower observations that are on the order of 1.26–1.47 nmol $\cdot$ $m^{-2} \cdot s^{-1}$ (Griffis et al., 2019). The dry deposition rate to forested lands was on the order of 0.13 $\pm$ 0.01 nmol $\cdot$ $m^{-2} \cdot s^{-1}$, and NH_3 NEE was -0.07 ± 0.01 nmol $\cdot$ $m^{-2} \cdot s^{-1}$. Note that for these simulations, we applied the derived NEI 2017 inventory without monthly variations. When considering monthly scaling factors 0.73, 1.02, 1.35, and 0.94 for February, May, August, and November, respectively, based on the EDGAR inventory, the simulated NH_3 mixing ratios were higher for May and August and lower in February. Assuming that the ground-level NH_3 mixing ratios follow this same monthly scaling, we recalculated the ground-level NH_3 mixing ratio and dry deposition as shown in Figures 9c and 9e (i.e., red line designates crop lands).

Based on the AMoN observations and modeled V_d for NH_3, Li et al. (2016) calculated an annual average NH_3 dry deposition of 1.27 nmol $\cdot$ $m^{-2} \cdot s^{-1}$ in the Upper Midwest. Our simulations for 2017 indicate that the dry deposition rate was 0.94 $\pm$ 0.02 nmol $\cdot$ $m^{-2} \cdot s^{-1}$ (0.97 $\pm$ 0.02 nmol $\cdot$ $m^{-2} \cdot s^{-1}$ after the monthly scaling recalculation) for agricultural lands, which is in excellent agreement with previous estimates. The ecosystem-dependent critical load (a quantitative value above which significant harmful effects on specified sensitive elements of the environment will occur) for nitrogen is estimated to be 2.5–5 kg N $\cdot$ $ha^{-1} \cdot year^{-1}$ (Ellis et al., 2013; Pardo et al., 2011). To estimate the nitrogen load in forested areas within our study domain, we combined our simulated NH_3 dry deposition (0.57 $\pm$ 0.04 kg N $\cdot$ $ha^{-1} \cdot year^{-1}$) with the findings by Li et al. (2016), who concluded that dry deposition of NH_3 contributed 19–65% across the United States. Our calculated total nitrogen deposition was 0.87–3.00 kg N $\cdot$ $ha^{-1} \cdot year^{-1}$, which is on average below the critical load of natural parks.

The seasonal variations in the dry deposition flux are driven by variations in both the deposition velocity and the NH_3 mixing ratio distributions. The simulated dry deposition velocity was 0.34 $\pm$ 0.001 cm/s (winter) and 0.37 $\pm$ 0.002 cm/s (autumn) and increased to 0.81 $\pm$ 0.005 cm/s (spring) and 0.73 $\pm$ 0.00 cm/s (summer) for crops. The dry deposition velocity was 0.34 $\pm$ 0.004 cm/s (winter) and 0.45 $\pm$ 0.004 cm/s (autumn) and increased to 0.55 $\pm$ 0.007 cm/s (spring) and 0.48 $\pm$ 0.007 cm/s (summer) for forested lands. The dry deposition flux ratios in spring and summer were much larger than winter and autumn (Figure 9f), resulting in more NH_3 deposition to forests in the cold season (Figure 9e). This large difference can be explained by two factors: (1) higher vertical turbulence in the warm season leads to higher PBL height and lower atmospheric NH_3 mixing ratios near the ground and (2) V_d in the warm season were higher than during the cold season, so that during the period of crop growth, more NH_3 was deposited near the emission sources with less subsequent atmospheric transport to northern forested areas. Previous studies also observed elevated dry NH_3 deposition in winter for the Upper Midwest area (Chen et al., 2014; Li et al., 2016), which was driven by relatively high winter NH_3 emissions from winter fertilizer application and livestock and combined with a relatively shallow PBL.

4. Conclusions

1. The derived NEI 2017 emission inventory showed better agreement with our tall tower observations than the other emission inventories (NEI 2011 and EDGAR), with mean bias (RMSE) of 0.54 (5.37) ppb and 0.71 (3.22) ppb in November, 2017 and 2018, respectively.
2. The regional temperature sensitivity (Q_{10}) of gross NH_3 emissions was estimated to be 2.5, indicating strong potential for significantly higher emissions under warmer conditions. Future warmer temperatures have potential to enhance agricultural N losses and increase dry deposition in downwind natural ecosystems.
3. Intensive livestock NH_3 emissions in northern Iowa were found to contribute up to 1.07 ppb of NH_3 at the tall tower site for November 2017, representing about 17.6% of simulated NH_3 mixing ratios.
4. NH_3 mixing ratios in domain 3 frequently exceeded (i.e., 336 hr, 48% of November 2017) the high risk air quality health standard of 5.3 ppb.
5. The domain-averaged NH_3 emissions showed a linear relationship with dry deposition ($y = 0.42x + 0.07$), where x and y indicate NH_3 emissions and dry deposition (nmol $\cdot$ m^{-2} $\cdot$ s^{-1}), respectively. This can be interpreted as the regional average dry deposition velocity (0.44 ± 0.01) for NH_3, and its intercept represents the dry deposition flux (0.06 nmol $\cdot$ m^{-2} $\cdot$ s^{-1}) resulting from long distance transport;
6. November NH_3 NEE accounted for 60.1–64.6% of gross NH_3 emissions for agricultural areas and was 2.8–3.1 times greater in magnitude than the gross emissions for forested areas. The simulated NH_3 NEE were 1.60 ± 0.06 nmol $\cdot$ m^{-2} $\cdot$ s^{-1} for agricultural lands and -0.07 ± 0.02 nmol $\cdot$ m^{-2} $\cdot$ s^{-1} for forests.

Acknowledgments
This research was partially supported by the National Science Foundation (grant 1640337), the U.S. Department of Agriculture National Institute of Food and Agriculture (USDA NIFA grant 2018-67019-27808), USDA Agricultural Research Service, and the Minnesota Supercomputing Institute for Advanced Computational Research. Jeffrey D. Wood acknowledges support from the U.S. Department of Energy, Office of Science, Office of Biological and Environmental Research Program, through Oak Ridge National Laboratory's Terrestrial Ecosystem Science Focus Area; ORNL is managed by UT-Battelle, LLC, for the U.S. DOE under contract DE-AC05-00OR22725. We acknowledge use of the National Atmospheric Deposition Program databases. Finally, the observational data presented in this manuscript are available at www.biometeorology.umn.edu/research/data-archives and ESS-DIVE (Deep Insights for Earth Science Data, https://data.ess-dive.lbl.gov/view/doi:10.15485/1550921). The NH_3 data can also be obtained from our group website https://www.biometeorology.umn.edu/research/data-archives. The WRF-Chem model code is available on https://www2.mmm.ucar.edu/wrf/users/download/. Finally, the WRF-CHEM setup parameters (namelist) are provided in the supporting information.

References

Ackermann, I. J., Hass, H., Memmesheimer, M., Ebel, A., Binkowski, F. S., & Shankar, U. (1998). Modal aerosol dynamics model for Europe: Development and first applications. *Atmospheric Environment*, *32*(17), 2981–2999. https://doi.org/10.1016/S1352-2310(98)00006-5

Andersen, H., Hovmand, M., Hummelshoj, P., & Jensen, N. O. (1993). Measurements of ammonia flux to a spruce stand in Denmark. *Atmospheric Environment*, *27A*, 189–202.

Andersen, H. V., Hovmand, M. F., Hummelsh, P., & Jensen, N. O. (1999). Measurements of ammonia concentrations, fluxes and dry deposition velocities to a spruce forest 1991–1995. *Atmospheric Environment*, *33*(9), 1367–1383. https://doi.org/10.1016/S1352-2310(98)00363-X

Aneja, V. P., Chauhan, J. P., & Walker, J. T. (2000). Characterization of atmospheric ammonia emissions from swine waste storage and treatment lagoons. *Journal of Geophysical Research*, *105*(D9), 11,535–11,545. https://doi.org/10.1029/2000JD900066

Bash, J. O., Cooter, E. J., Dennis, R. L., Walker, J. T., & Pleim, J. E. (2013). Evaluation of a regional airquality model with bidirectional NH_3 exchange coupled to an agroecosystem model. *Biogeosciences*, *10*(3), 1635–1645. https://doi.org/10.5194/bg-10-1635-2013

Battye, W. H., Bray, C. D., Aneja, V. P., Tong, D., & Lee, P. (2016). Evaluating ammonia (NH 3) predictions in the NOAA National Air Quality Forecast Capability (NAQFC) using in situ aircraft, ground-level, and satellite measurements from the DISCOVER-AQ Colorado campaign. *Atmospheric Environment*, *140*, 342–351. https://doi.org/10.1016/j.atmosenv.2016.06.021

Butler, T., Vermeylen, F., Lehmann, C. M., Likens, G. E., & Puchalski, M. (2016). Increasing ammonia concentration trends in large regions of the USA derived from the NADP/AMoN network. *Atmospheric Environment*, *146*(3), 132–140. https://doi.org/10.1016/j.atmosenv.2016.06.033

Butler, T., Marino, R., Schwede, D., Howarth, R., Sparks, J., & Sparks, K. (2015). Atmospheric ammonia measurements at low concentration sites in the northeastern USA: Implications for total nitrogen deposition and comparison with CMAQ estimates. *Biogeochemistry*, *122*(2-3), 191–210. https://doi.org/10.1007/s10533-014-0036-5

Chen, X., Day, D., Schichtel, B., Malm, W., Matzoll, A. K., Mojica, J., et al. (2014). Seasonal ambient ammonia and ammonium concentrations in a pilot IMPROVE NHx monitoring network in the western United States. *Atmospheric Environment*, *91*, 118–126. https://doi.org/10.1016/j.atmosenv.2014.03.058

Chen, Z., Grif, T. J., Millet, D. B., Wood, J. D., Lee, X., Baker, J. M., et al. (2016). Global biogeochemical cycles. AGU Publication Water Resources Research, 1192–1205. https://doi.org/10.1002/2015GB005313.Received

Chen, Z., Griffis, T. J., Baker, J. M., Millet, D. B., Wood, J. D., Dlugokencky, E. J., et al. (2018). Source partitioning of methane emissions and its seasonality in the U.S. Midwest. *Journal of Geophysical Research: Biogeosciences*, *123*, 646–659. https://doi.org/10.1002/2017JG004356

Chu, K., Peng, Z., Liu, Z., Lei, L., Kou, X., Zhang, Y., et al. (2018). Evaluating the impact of emissions regulations on the emissions reduction during the 2015 China Victory Day parade with an ensemble square root filter. *Journal of Geophysical Research: Atmospheres*, *123*, 4122–4134. https://doi.org/10.1002/2017JD027631

Cooter, E. J., Bash, J. O., Benson, V., & Ran, L. (2012). Linking agricultural crop management and air quality models for regional to national-scale nitrogen assessments. *Biogeosciences*, *9*, 4023–4035. https://doi.org/10.5194/bg-9-4023-2012

Dammers, E., Schaap, M., Haaima, M., Palm, M., Wichink Kruit, R. J., Volten, H., et al. (2017). Measuring atmospheric ammonia with remote sensing campaign: Part 1—Characterisation of vertical ammonia concentration profile in the centre of The Netherlands. *Atmospheric Environment*, *169*, 97–112. https://doi.org/10.1016/j.atmosenv.2017.08.067

Dragosits, U., Theobald, M. R., Place, C. J., Lord, E., Webb, J., Hill, J., et al. (2002). Ammonia emission, deposition and impact assessment at the field scale: A case study of sub-grid spatial variability. *Environmental Pollution*, *117*(1), 147–158. https://doi.org/10.1016/S0269-7491(01)00147-6

Duyzer, J. H., Verhagen, H. L. M., Weststrate, J. H., & Bosveld, F. C. (1992). Measurement of the dry deposition flux of nh3 on to coniferous forest. *Environmental Pollution*, *75*(1), 3–13.

Ellis, R. A., Jacob, D. J., Sulprizio, M. P., Zhang, L., Holmes, C. D., Schichtel, B. A., et al. (2013). Present and future nitrogen deposition to national parks in the United States: critical load exceedances. *Atmospheric Chemistry and Physics*, *13*, 9083–9095. https://doi.org/10.5194/acp-13-9083-2013

Erisman, J. W., Sutton, M. A., Galloway, J., Klimont, Z., & Winiwarter, W. (2008). How a century of ammonia synthesis changed the world. *Nature Geoscience*, *1*(10), 636.

Ferrara, R. M., Loubet, B., di Tommasi, P., Bertolini, T., Magliulo, V., Cellier, P., et al. (2012). Eddy covariance measurement of ammonia fluxes: Comparison of high frequency correction methodologies. *Agricultural and Forest Meteorology*, *158-159*, 30–42. https://doi.org/10.1016/j.agrformet.2012.02.001

Ferrara, R. M., Carozzi, M., Di Tommasi, P., Nelson, D. D., Fratini, G., Bertolini, T., et al. (2016). Dynamics of ammonia volatilisation measured by eddy covariance during slurry spreading in north Italy. *Agriculture, Ecosystems and Environment*, *219*, 1–13. https://doi.org/10.1016/j.agee.2015.12.002

Fu, C., Lee, X., Griffis, T. J., Dlugokencky, E. J., & Andrews, A. E. (2017). Investigation of the N2O emission strength in the U. S. Corn Belt. *Atmospheric Research*, *194*(January), 66–77. https://doi.org/10.1016/j.atmosres.2017.04.027

Galloway, J. N., Townsend, A. R., Erisman, J. W., Bekunda, M., Cai, Z., Freney, J. R., et al. (2008). Transformation of the nitrogen cycle: Recent trends, questions, and potential solutions. *Science*, *320*(5878), 889–892. https://doi.org/10.1126/science.1136674

Griffis, T. J., Baker, J. M., Sargent, S. D., Erickson, M., Corcoran, J., Chen, M., & Billmark, K. (2010). Influence of C4 vegetation on 13CO2 discrimination and isoforcing in the upper Midwest, United States. *Global Biogeochemical Cycles*, *24*, GB4006. https://doi.org/10.1029/2009GB003768

Griffis, T. J., Hu, C., Baker, J. M., Wood, J. D., Millet, D. B., Erickson, M., et al. (2019). Tall tower ammonia observations and emission estimates in the US Midwest. *Journal of Geophysical Research: Biogeosciences*, *124*, 3432–3447. https://doi.org/10.1029/2019JG005172

Griffis, T. J., Lee, X., Baker, J. M., Russelle, M. P., Zhang, X., Venterea, R., & Millet, D. B. (2013). Reconciling the differences between top-down and bottom-up estimates of nitrous oxide emissions for the U.S. Corn Belt. *Global Biogeochemical Cycles*, *27*, 746–754. https://doi.org/10.1002/gbc.20066

Griffis, T. J., Wood, J. D., Baker, J. M., Lee, X., Xiao, K., Chen, Z., et al. (2016). Investigating the source, transport, and isotope composition of water vapor in the planetary boundary layer. *Atmospheric Chemistry and Physics*, *16*(8), 5139–5157. https://doi.org/10.5194/acp-16-5139-2016

Griffis, T. J., Chen, Z., Baker, J. M., Wood, J. D., Millet, D. B., Lee, X., et al. (2017). Nitrous oxide emissions are enhanced in a warmer and wetter world. *Proceedings of the National Academy of Sciences*, *114*(45), 12,081–12,085. https://doi.org/10.1073/pnas.1704552114

Heald, C. L., Collett, J. L. Jr., Lee, T., Benedict, K. B., Schwandner, F. M., Li, Y., et al. (2012). Atmospheric ammonia and particulate inorganic nitrogen over the United States. *Atmospheric Chemistry and Physics*, *12*(21), 10,295–10,312. https://doi.org/10.5194/acp-12-10295-2012

Hellsten, S., Dragosits, U., Place, C. J., Vieno, M., Dore, A. J., Misselbrook, T. H., et al. (2008). Modelling the spatial distribution of ammonia emissions in the UK. *Environmental Pollution*, *154*(3), 370–379. https://doi.org/10.1016/j.envpol.2008.02.017

Hensen, A., Loubet, B., Mosquera, J., Bulk, W. C. M. V. D., Erisman, J. W., Dämmgen, U., et al. (2009). Estimation of nh3 emissions from a naturally ventilated livestock farm using local-scale atmospheric dispersion modelling. *Biogeosciences*, *6*(1), 2847–2860.

Hu, C., Griffis, T. J., Lee, X., Millet, D. B., Chen, Z., Baker, J. M., & Xiao, K. (2018). Top-down constraints on anthropogenic CO_2 emissions within an agricultural-urban landscape. *Journal of Geophysical Research: Atmospheres*, *123*, 4674–4694. https://doi.org/10.1029/2017JD027881

Hu, L., Millet, D. B., Baasandorj, M., Grif, T. J., Turner, P., Helmig, D., et al. (2015). Isoprene emissions and impacts over an ecological transition region in the US Upper Midwest inferred from tall tower measurements. *Journal of Geophysical Research: Atmospheres*, *120*, 3553–3571. https://doi.org/10.1002/2014JD022732.Received

Hu, X. M., Klein, P. M., Xue, M., Shapiro, A., & Nallapareddy, A. (2013). Enhanced vertical mixing associated with a nocturnal cold front passage and its impact on near-surface temperature and ozone concentration. *Journal of Geophysical Research: Atmospheres*, *118*, 2714–2728. https://doi.org/10.1002/jgrd.50309

Intergovernmental Panel on Climate Change (IPCC) (2013). Climate change 2013: The physical science basis, contribution of Working Group I to the Fifth Assessment Report of the Intergovernmental Panel on Climate Change. Cambridge: Cambridge University Press.

Kelleghan, D. B., Hayes, E. T., Everard, M., & Curran, T. P. (2019). Science of the total environment mapping ammonia risk on sensitive habitats in Ireland. *Science of the Total Environment*, *649*, 1580–1589. https://doi.org/10.1016/j.scitotenv.2018.08.424

Kim, S. Y., Millet, D. B., Hu, L., Mohr, M. J., Griffis, T. J., Wen, D., et al. (2013). Constraints on carbon monoxide emissions based on tall tower measurements in the U.S. upper midwest. *Environmental Science and Technology*, *47*(15), 8316–8324. https://doi.org/10.1021/es4009486

Lebel, P. J., Hoell, J. M., Levine, J. S., & Vay, S. A. (1985). Aircraft measurements of ammonia and nitric acid in the lower troposphere. *Geophysical Research Letters*, *12*(6), 401–404. https://doi.org/10.1029/GL012i006p00401

Li, Y., Schichtel, B. A., Walker, J. T., Schwede, D. B., Chen, X., Lehmann, C. M. B., et al. (2016). Increasing importance of deposition of reduced nitrogen in the United States. *Proceedings of the National Academy of Sciences*, *113*(21), 5874–5879. https://doi.org/10.1073/pnas.1525736113

Li, Y., Thompson, T. M., van Damme, M., Chen, X., Benedict, K. B., Shao, Y., et al. (2017). Temporal and spatial variability of ammonia in urban and agricultural regions of northern Colorado, United States. *Atmospheric Chemistry and Physics*, *17*(10), 6197–6213. https://doi.org/10.5194/acp-17-6197-2017

Lonsdale, C. R., Hegarty, J. D., Cady-Pereira, K. E., Alvarado, M. J., Henze, D. K., Turner, M. D., et al. (2017). Modeling the diurnal variability of agricultural ammonia in Bakersfield, California, during the CalNex campaign. *Atmospheric Chemistry and Physics*, *17*(4), 2721–2739. https://doi.org/10.5194/acp-17-2721-2017

Lv, J., Buerkert, A., Benedict, K. B., Liu, G., Lv, C., & Liu, X. (2019). Comparison of nitrogen deposition across different land use types in agro-pastoral catchments of western china and mongolia. *Atmospheric Environment*, *199*, 313–322.

Makar, P. A., Gong, W., Hogrefe, C., Zhang, Y., Curci, G., Žabkar, R., et al. (2015). Feedbacks between air pollution and weather. Part 2: Effects on chemistry. *Atmospheric Environment*, *115*, 499–526. https://doi.org/10.1016/j.atmosenv.2014.10.021

McGinn, S. M., Flesch, T. K., Crenna, B. P., Beauchemin, K. A., & Coates, T. (2007). Quantifying ammonia emissions from a cattle feedlot using a dispersion model. *Journal of Environmental Quality*, *36*(6), 1585. https://doi.org/10.2134/jeq2007.0167

NADP (2017). Ammonia Monitoring Network (AMoN), National Atmospheric Deposition Program (NRSP-3). 2017. Champaign, IL: NADP Program Office, Illinois State Water Survey, University of Illinois. Retrieved from http://nadp.sws.uiuc.edu/AMoN/

Nelson, A. J., Koloutsou-Vakakis, S., Rood, M. J., Myles, L. T., Lehmann, C., Bernacchi, C., et al. (2017). Agricultural and Forest Meteorology Season-long ammonia flux measurements above fertilized corn in central Illinois, USA, using relaxed eddy accumulation. *Agricultural and Forest Meteorology*, *239*, 202–212. https://doi.org/10.1016/j.agrformet.2017.03.010

Nelson, A. J., Lichiheb, N., Koloutsou-Vakakis, S., Rood, M. J., Heuer, M., Myles, L. T., et al. (2019). Agricultural and forest meteorology ammonia flux measurements above a corn canopy using relaxed eddy accumulation and a flux gradient system. *Agricultural and Forest Meteorology*, *264*(October 2018), 104–113. https://doi.org/10.1016/j.agrformet.2018.10.003

Nowak, J. B., Neuman, J. A., Bahreini, R., Middlebrook, A. M., Holloway, J. S., Mckeen, S. A., et al. (2012). Ammonia sources in the california south coast air basin and their impact on ammonium nitrate formation. *Geophysical Research Letters*, *39*(7), 102–114.

Oleson, K. W., Lawrence, D. M., Gordon, B., Flanner, M. G., Kluzek, E., Peter, J., et al. (2013). Technical description of version 4.5 of the Community Land Model (CLM), NCAR/TN-503+STR NCAR Tech. Note, (July) (266 pp.). https://doi.org/10.5065/D6RR1W7M

Olivier, J. G. J., Bouwman, A. F., Van der Maas, C. W. M., & Berdowski, J. J. M. (1994). Emission Database for Global Atmospheric Research (EDGAR). *Environmental Monitoring and Assessment*, *31*(1-2), 93–106.

Pardo, L. H., Fenn, M. E., Goodale, C. L., Geiser, L. H., Driscoll, C. T., Allen, E. B., et al. (2011). Effects and empirical critical loads of nitrogen for ecoregions of the united effects of nitrogen deposition and empirical nitrogen critical loads for ecoregions of the United States. *Ecological Applications*, *21*(8), 3049–3082. https://doi.org/10.1007/978-94-017-9508-1

Parker, D., Ham, J., Woodbury, B., Cai, L., Spiehs, M., Rhoades, M., et al. (2013). Standardization of flux chamber and wind tunnel flux measurements for quantifying volatile organic compound and ammonia emissions from area sources at animal feeding operations. *Atmospheric Environment*, *66*, 72–83. https://doi.org/10.1016/j.atmosenv.2012.03.068

Paulot, F., Jacob, D. J., Pinder, R. W., Bash, J. O., Travis, K., & Henze, D. K. (2014). Ammonia emissions in the United States, European Union, and China derived by high-resolution inversion of ammonium wet deposition data: Interpretation with a new agricultural emissions inventory (MASAGE_NH3). *Journal of Geophysical Research: Atmospheres*, *119*, 4343–4364. https://doi.org/10.1002/2013JD021130

Phillips, S. B., Arya, S. P., & Aneja, V. P. (2004). Ammonia flux and dry deposition velocity from near-surface concentration gradient measurements over a grass surface in North Carolina. *Atmospheric Environment*, *38*(21), 3469–3480. https://doi.org/10.1016/j.atmosenv.2004.02.054

Pleim, J. E., Bash, J. O., Walker, J. T., & Cooter, E. J. (2013). Development and evaluation of an ammonia bidirectional flux parameterization for air quality models. *Journal of Geophysical Research: Atmospheres*, *118*, 3794–3806.

Pryor, S. C., Barthelmie, R. J., Sørensen, L. L., & Jensen, B. (2001). Ammonia concentrations and fluxes over a forest in the midwestern USA. *Atmospheric Environment*, *35*(32), 5645–5656. https://doi.org/10.1016/S1352-2310(01)00259-X

Puchalski, M. A., Rogers, C. M., Baumgardner, R., Mishoe, K. P., Price, G., Smith, M. J., & Lehmann, C. M. (2015). Environmental Science A statistical comparison of active and passive ammonia measurements collected at Clean Air Status and Trends Network (CASTNET) sites. *Environmental Science: Processes & Impacts*, *17*(2), 358–369. https://doi.org/10.1039/c4em00531g

Puchalski, M. A., Sather, M. E., Walker, J. T., Lehmann, C. M. B., Gay, D. A., Mathew, J., & Robarge, W. P. (2011). Passive ammonia monitoring in the United States: Comparing three different Passive ammonia monitoring in the United States: Comparing three different sampling devices †. *Journal of Environmental Monitoring*, *13*(11), 3156–3167. https://doi.org/10.1039/c1em10553a

Reis, S., Pinder, R. W., Zhang, M., Lijie, G., & Sutton, M. A. (2009). Reactive nitrogen in atmospheric emission inventories. *Atmospheric Chemistry and Physics*, *9*(19), 7657–7677. https://doi.org/10.5194/acp-9-7657-2009

Riddick, S., Ward, D., Hess, P., Mahowald, N., Massad, R., & Holland, E. (2016). Estimate of changes in agricultural terrestrial nitrogen pathways and ammonia emissions from 1850 to present in the Community Earth System Model. *Biogeosciences*, *13*(11), 3397. https://doi.org/10.5194/bg-13-3397-2016

Rose, L. A., Sebestyen, S. D., Elliott, E. M., & Koba, K. (2015). Drivers of atmospheric nitrate processing and export in forested catchments. *Water Resources Research*, *51*, 1333–1352. https://doi.org/10.1002/2014WR015716

Schell, B., Ackermann, I. J., Hass, H., Binkowski, F. S., & Ebel, A. (2001). Modeling the formation of secondary organic aerosol within a comprehensive air quality model system. *Journal of Geophysical Research*, *106*(D22), 28,275–28,293. https://doi.org/10.1029/2001JD000384

Schrader, F., Schaap, M., Zöll, U., Kranenburg, R., & Brümmer, C. (2018). The hidden cost of using low-resolution concentration data in the estimation of NH 3 dry deposition fluxes. *Scientific Reports*, *8*(1), 969. https://doi.org/10.1038/s41598-017-18021-6

Sebestyen, S. D., Shanley, J. B., Boyer, E. W., Kendall, C., & Doctor, D. H. (2014). Coupled hydrological and biogeochemical processes controlling variability of nitrogen species in streamflow during autumn in an upland forest. *Water Resources Research*, *50*, 1569–1591. https://doi.org/10.1002/2013WR013670

Sebestyen, S. D., Ross, D. S., Shanley, J. B., Elliott, E. M., Kendall, C., Campbell, J. L., et al. (2019). Unprocessed atmospheric nitrate in waters of the northern forest region in the U.S. and. *Canada Environmental Science & Technology*, *53*(7), 3620–3633. https://doi.org/10.1021/acs.est.9b01276

Shephard, M. W., Cady-Pereira, K. E., Luo, M., Henze, D. K., Pinder, R. W., Walker, J. T., et al. (2011). TES ammonia retrieval strategy and global observations of the spatial and seasonal variability of ammonia. *Atmospheric Chemistry and Physics*, *11*(20), 10,743–10,763. https://doi.org/10.5194/acp-11-10743-2011

Skjøth, C. A., & Geels, C. (2013). The effect of climate and climate change on ammonia emissions in Europe. *Atmospheric Chemistry and Physics*, *13*(1), 117–128. https://doi.org/10.5194/acp-13-117-2013

Stevens, C. J. (2019). Nitrogen in the environment. *Science*, *363*(6427), 578–580. https://doi.org/10.1126/science.aav8215

Stockwell, W. R., Middleton, P., Chang, J. S., & Tang, X. (1990). The second generation regional acid deposition model chemical mechanism for regional air quality modeling. *Journal of Geophysical Research*, *95*(D10), 16,343. https://doi.org/10.1029/JD095iD10p16343

Sun, K., Tao, L., Miller, D. J., Zondlo, M. A., Shonkwiler, K. B., Nash, C., & Ham, J. M. (2015). Open-path eddy covariance measurements of ammonia fluxes from a beef cattle feedlot. *Agricultural and Forest Meteorology*, *213*, 193–202. https://doi.org/10.1016/j.agrformet.2015.06.007

Sutton, M. A., Reis, S., Riddick, S. N., Dragosits, U., Nemitz, E., Theobald, M. R., et al. (2013). Towards a climate-dependent paradigm of ammonia emission and deposition. *Philosophical Transactions of the Royal Society, B: Biological Sciences*, *368*(1621). https://doi.org/10.1098/rstb.2013.0166

Tevlin, A. G., Li, Y., Collett, J. L., McDuffie, E. E., Fischer, E. V., & Murphy, J. G. (2017). Tall tower vertical profiles and diurnal trends of ammonia in the Colorado Front Range. *Journal of Geophysical Research: Atmospheres*, *122*, 12,468–12,487. https://doi.org/10.1002/2017JD026534

Tuccella, P., Curci, G., Visconti, G., Bessagnet, B., Menut, L., & Park, R. J. (2012). Modeling of gas and aerosol with WRF/Chem over Europe: Evaluation and sensitivity study. *Journal of Geophysical Research*, *117*, D03303. https://doi.org/10.1029/2011JD016302

Warner, J. X., Dickerson, R. R., Wei, Z., Strow, L. L., Wang, Y., & Liang, Q. (2017). Increased atmospheric ammonia over the world's major agricultural areas detected from space. *Geophysical Research Letters*, *44*, 2875–2884. https://doi.org/10.1002/2016GL072305

Wesely, M. L. (1989). Parameterization of surface resistances to gaseous dry deposition in regional-scale numerical models *. *Atmospheric Environment*, *23*(6), 1293–1304. https://doi.org/10.1016/0004-6981(89)90153-4

Whaley, C. H., Makar, P. A., Shephard, M. W., Zhang, L., Zhang, J., Zheng, Q., et al. (2018). Contributions of natural and anthropogenic sources to ambient ammonia in the Athabasca Oil Sands and north-western Canada. *Atmospheric Chemistry and Physics*, *18*(3), 2011–2034. https://doi.org/10.5194/acp-18-2011-2018

Wu, Z., Wang, X., Chen, F., Turnipseed, A. A., Guenther, A. B., Niyogi, D., et al. (2011). Evaluating the calculated dry deposition velocities of reactive nitrogen oxides and ozone from two community models over a temperate deciduous forest. *Atmospheric Environment*, *45*(16), 2663–2674. https://doi.org/10.1016/j.atmosenv.2011.02.063

Yang, Y., Liao, W., Wang, X., Liu, C., Xie, Q., Gao, Z., et al. (2016). Quantification of ammonia emissions from dairy and beef feedlots in the Jing-Jin-Ji district, China. *Agriculture, Ecosystems and Environment*, *232*, 29–37. https://doi.org/10.1016/j.agee.2016.07.016

Yegorova, E. A., Allen, D. J., Loughner, C. P., Pickering, K. E., & Dickerson, R. R. (2011). Characterization of an eastern U. S. severe air pollution episode using WRF/Chem. *Journal of Geophysical Research*, *116*, D17306. https://doi.org/10.1029/2010JD015054

Yu, F., Nair, A. A., & Luo, G. (2018). Long-term trend of gaseous ammonia over the United States: Modeling and comparison with observations. *Journal of Geophysical Research: Atmospheres*, *123*, 8315–8325. https://doi.org/10.1029/2018JD028412

Zhang, L., Jacob, D. J., Knipping, E. M., Kumar, N., Munger, J. W., Carouge, C. C., & van Donkelaar, A. (2012). Nitrogen deposition to the United States: Distribution, sources, and processes. *Atmospheric Chemistry and Physics*, *12*(10), 4539–4554. https://doi.org/10.5194/acp-12-4539-2012

Zhang, X., Lee, X., Griffis, T. J., Baker, J. M., & Xiao, W. (2014). Estimating regional greenhouse gas fluxes: An uncertainty analysis of planetary boundary layer techniques and bottom-up inventories. *Atmospheric Chemistry and Physics*, *14*(19), 10,705–10,719. https://doi.org/10.5194/acp-14-10705-2014

Zhang, X., Wu, Y., Liu, X., Reis, S., Jin, J., Dragosits, U., et al. (2017). Ammonia emissions may be substantially underestimated in China. *Environmental Science and Technology*, *51*(21), 12,089–12,096. https://doi.org/10.1021/acs.est.7b02171

Zhang, Y., Tang, A., Wang, D., Wang, Q., Benedict, K., Zhang, L., & Liu, D. (2018). The vertical variability of ammonia in urban Beijing, China. *Atmospheric Chemistry and Physics*, *18*(22), 16,385–16,398. https://doi.org/10.5194/acp-18-16385-2018

Zhu, L., Henze, D. K., Cady-Pereira, K. E., Shephard, M. W., Luo, M., Pinder, R. W., et al. (2013). Constraining U.S. ammonia emissions using TES remote sensing observations and the GEOS-Chem adjoint model. *Journal of Geophysical Research: Atmospheres*, *118*, 3355–3368. https://doi.org/10.1002/jgrd.50166

Zhu, L., Henze, D. K., Bash, J. O., Cady-Pereira, K. E., Shephard, M. W., Luo, M., & Capps, S. L. (2015). Sources and impacts of atmospheric NH_3: Current understanding and frontiers for modeling, measurements, and remote sensing in North America. *Current Pollution Reports*, *1*(2), 95–116. https://doi.org/10.1007/s40726-015-0010-4

Zhu, S., Horne, J. R., Montoya-Aguilera, J., Hinks, M. L., & Nizkorodov, S. A. (2018). Modeling reactive ammonia uptake by secondary organic aerosol in CMAQ: application to the continental US. *Atmospheric Chemistry and Physics*, *18*(5), 3641–3657.

Zhu, T., Pattey, E., & Desjardins, R. L. (2000). Relaxed eddy-accumulation technique for measuring ammonia volatilization. *Environmental Science & Technology*, *34*(1), 199–203. https://doi.org/10.1021/es980928f